Title
Digitally Enhanced Switched-Mode RF Transmitters for Efficiency, Bandwidth and Fidelity

Author
Zhu, Rui

Publication Date
2017

Peer reviewed|Thesis/dissertation

UNIVERSITY OF CALIFORNIA

Los Angeles

Digitally Enhanced Switched-Mode RF Transmitters for Efficiency, Bandwidth and Fidelity

A dissertation submitted in partial satisfaction
of the requirements for the degree
Doctor of Philosophy in Electrical Engineering

by

Rui Zhu

2017

ABSTRACT OF THE DISSERTATION

Digitally Enhanced Switched-Mode RF Transmitters
for Efficiency, Bandwidth and Fidelity

by

Rui Zhu
Doctor of Philosophy in Electrical Engineering
University of California, Los Angeles, 2017
Professor Yuanxun Wang, Chair

Power efficiency, bandwidth, and signal fidelity are critical specs of wireless transmitters, which are often traded off in transmitters with conventional analog circuit and antenna design. For example, high quality factor antennas and components help to achieve high efficiencies but often suffer bandwidth limitations. Switched-mode amplifiers and antennas have been proposed to achieve both high efficiency and broad bandwidth but the quantization noise issues prevent those techniques from being practically deployed.

In this research, digitally enhanced techniques are proposed to enhance the design of switched-mode RF transmitter toward higher data rates, better power efficiency and lower quantization noise. Two specific research projects will be discussed. In the first project, an active noise filtering technique called Channelized Active Noise Elimination (CANE) is used to actively suppress the quantization noise in the bitstream modulated transmitter by employing the delaying and combining structure of multiple power amplification channels. The power efficiency of each of the power amplifier is preserved by a load modulation mechanism in the power combining operation. The proposed technique is implemented in a transmitter with a FPGA based signal processing module and the experimental results prove that the CANE technique can be a software-controlled, robust and flexibly tunable filter solution.

The second project is utilizing the Direct Antenna Modulation (DAM) technique to surpass the physical bandwidth limit imposed by the high radiation quality factor of the

electrically small antenna. The DAM concept has been proposed with various types of digital modulations, such as On/Off Keying, BPSK and QPSK, etc. A newly proposed DAM frequency shift keying (FSK) is developed to synthesize the parasitic components of switches with the matching circuit to improve the switching quality and signal integrity in the switched-mode electrically small antenna system.

The dissertation of Rui Zhu is approved.

Tatsuo Itoh

Gregory P Carman

Yuanxun Wang, Committee Chair

University of California, Los Angeles

2017

To my Families, Friends, Colleagues and Advisor

TABLE OF CONTENTS

LIST OF FIGURES

LIST OF TABLES

ACKNOWLEDGMENTS

First and foremost, I would like to thank my advisor, Prof. Yuanxun Ethan Wang, for his guidance, patience, inspiration and all the other support throughout my PhD career.

I would also like to express my thank to Prof. Tatsuo Itoh, Prof. Sudhakar Pamarti and Prof. Greg Carman for taking time to serve on my dissertation committee.

Thanks to all of my Digital Microwave Lab fellows for those ideas, discussion and support in the past years. I have to say I am very lucky to meet the these geniuses.

Thanks to Yueqin for supporting me.

Thanks to all my friends.

At last, I would like to express my greatest gratitude to my parents for offering me a wonderful life.

VITA

2007–2011 B.E. (Electronic Engineering), Tsinghua University, Beijing, China

2011–2013 M.S (Electrical Engineering), University of California, Los Angels, USA

2013-Present PhD Research Assistant, Electrical Engineering Department, University of California, Los Angels, USA

PUBLICATIONS

R.Zhu, Y.Song, and Y.E.Wang. "Suppressing transmitter intermodulations with Channelized Active Noise Elimination (CANE)." Microwave Symposium (IMS), 2015 IEEE MTT-S International. IEEE, 2015.

R.Zhu, Y.Song, and Y.E.Wang. "A S-band bitstream transmitter with Channelized Active Noise Elimination (CANE)." Wireless and Microwave Technology Conference (WAMICON), 2015 IEEE 16th Annual. IEEE, 2015.

R.Zhu, Y.Song, and Y.E.Wang. "Channelized Active Noise Elimination (CANE) with envelope Delta Sigma modulation." Silicon Monolithic Integrated Circuits in RF Systems (SiRF), 2015 IEEE 15th Topical Meeting on. IEEE, 2015.

R.Zhu, Y.Song, and Y.E.Wang "Tunable RF Bandpass Filter for Interference Suppression in Software Defined Radios." Microwave Symposium (IMS), 2017 IEEE MTT-S International. IEEE, 2017.

R.Zhu, Y.Song, and Y.E.Wang. "A modified QPSK modulation technique for direct antenna modulation (DAM) systems." Antennas and Propagation Society International Symposium (APSURSI), 2014 IEEE. IEEE, 2014.

R.Zhu, and Y.E.Wang, et al. "Frequency Shift Keying for Direct Antenna Modulation (DAM) with Electrically Small Antenna." Antennas and Propagation Society International Symposium (APSURSI), 2014 IEEE. IEEE, 2014.

Y.Song, R. Zhu, and Y.E.Wang. "Active Noise Filtering for X-band GaN Transmitters with Bitstream Modulations." IEEE Transactions on Microwave Theory and Techniques (2017).

Y.Song, R. Zhu, and Y.E.Wang. "An X-Band Pulsed Load Modulation Transmitter with Multilevel Envelope DeltaSigma Modulations." IEEE Transactions on Microwave Theory and Techniques 64.11 (2016): 3643-3653.

Y.Song, R. Zhu, and Y.E.Wang. "A X-band GaN power amplifier with Bitstream modulations and active noise filtering." Microwave Symposium (IMS), 2015 IEEE MTT-S International. IEEE, 2015.

Y.Song, R. Zhu, and Y.E.Wang. "A pulsed load modulation (PLM) power amplifier with 3-level envelope delta-sigma modulation (EDSM)." Power Amplifiers for Wireless and Radio Applications (PAWR), 2015 IEEE Topical Conference on. IEEE, 2015.

M.Biedka, R.Zhu, Q.M.Xu and Y.E.Wang, "Ultra-Wide Band Non-reciprocity through Sequentially-Switched Delay Lines." Scientific reports 7 (2017): 40014.

CHAPTER 1

Introduction

In wireless transmitter design, fast data transferring speed and high power efficiency are two most fundamental requirements. According to Shannon's theorem, the channel capacity of a communication link is determined by its bandwidth and signal to noise ratio (SNR). Therefore, the transmitter has to send out signals with sufficient fidelity over a broad bandwidth. On the other hand, the data transmission is also requested to be power efficient to reduce the system cost. However, the power efficiency, bandwidth and signal fidelity cannot always reach to their optimum condition simultaneously in conventional transmitter architecture, and are often traded-off with conventional analogue circuit and antenna design due to some fundamental limitations. For example, conventional PA can achieve promising power efficiency at its peak output power, but the linearity is sacrificed as the transistors are driven into saturation region. However, as wireless communication system nowadays employs complicated modulation techniques to achieve higher spectral efficiency, the increasing Peak to Average Power Ratio (PAPR) brings stringent linearity requirement of the PA. So the PA output power has to be backed-off to a linear region where the power efficiency is not optimal. So PA designers usually have to make a balance between the efficiency and the linearity. Another example of limitation in transmitter is that the bandwidth of an electrically small antenna (ESA) system is intrinsically narrow because of its high radiation quality factor Q_{rad}. As the product of bandwidth and radiation efficiency of such antennas is inversely proportional to Q_{rad}, the conventional ESA system cannot transmit broadband signal efficiently.

To solve these dilemmas, switched-mode transmitter architectures have been proposed [1–10]. The bitstream modulated transmitter has been developed to amplify RF signal with

high efficiency while preserving signal linearity simultaneously. For example, envelope delta sigma modulation (EDSM) transmitter converts the non-constant envelope signal to have a bitstream type of envelope which can be amplified by switching mode PA efficiently, while the original signal linearity is preserved by its noise shaping function. Previous works prove that the bitstream modulated transmitter indeed offers a solution to break the efficiency and linearity dilemma. However, the quantization noise generated in the bitstream modulation needs to be sufficiently suppressed, otherwise such transmitter cannot be practically used. Previously, people proposed active noise filter to help suppress the quantization noise. But these active filters is not robust to the circuit variations and the system power efficiency degrades after filtering [11–15]. Switched-Mode electrically small antenna using Direct Antenna Modulation (DAM) [33–37] technique has been proposed to surpass the bandwidth limitation imposed by the high radiation quality factor. The DAM system utilizes switches to directly modulate the signal on the antenna with decoupling the radiating power and stored energy. As no fundamental energy dissipation in the switching operation, the DAM system can efficiently transmit a broadband signal whose symbol rate is much greater than the physical bandwidth. However, the stringent switching conditions required by DAM prevent higher order digital modulation scheme from being directly applied. In addition, the imperfection of switches brings great challenges in the implementation of DAM.

In this research, digital techniques are proposed to enhance the design of switched-mode RF transmitter towards higher data rates, better power efficiency and signal fidelity. Two specific research topics will be discussed to solve the issues mentioned above. In the first project, we propose an advanced active noise filtering technique called Channelized Active Noise Elimination (CANE) [16–18] to improve the quantization noise suppression in bitstream modulated transmitter. The CANE technique utilizes a combining effect of multiple baseband-delayed power amplification channels to emulate an active Finite Impulse Response (FIR) filter for suppressing the quantization noise at RF, with preserving the system power efficiency by a load modulation mechanism through the power combining operation. In the second project, various types of digital modulation scheme, such as Quadrature Phase Shift Keying (QPSK) and Frequency Shift Keying (FSK), have been adjusted to meet the switch-

ing condition in DAM system. In addition, a modified Binary FSK modulation scheme is proposed in DAM system to help improve the switching quality.

In this thesis, we summarize the theorem, simulation, implementation and experimental results of proposed digitally enhanced switched mode transmitter. The rest of this article has two major parts. The first part includes Chapter 2 and Chapter 3, in which bitstream modulated transmitter and CANE technique will be discussed. Chapter II will introduce the concept and development of bitstream modulated transmitter. Chapter 3 will discuss the CANE technique with theory, simulation and experiment. The second part includes Chapter 4 and Chapter 5, in which switched mode electrically small antenna using DAM will be discussed. Chapter 4 will review the theory of the DAM. The development of DAM then will be discussed in Chapter 5. Finally, Chapter 6 will draw a conclusion of this research.

CHAPTER 2

Bitstream Modulated Switched-Mode transmitter

2.1 Efficiency and Linearity Enhancement

Nowadays complicated modulation techniques are widely used in wireless communication system to fully utilize the limited bandwidth resources. However, the PAPR of the signal is usually increased and brings difficulties in the high efficiency power amplifier design. In conventional power amplifier scheme, the power efficiency is usually proportional to the output power and the optimum efficiency often appears at the peak output power region, where the transistors are driven into saturation mode. With development of the semi-conductor devices, a decent optimum power efficiency is not difficult to achieve. However, with high PAPR signal, the average output power draws back to a much lower level with severe degradation of efficiency. Although the PA can be over-driven to obtain better efficiency performances, but the nonlinear distortions make it unusable in real application.

Many efficiency enhancement techniques have been developed to optimize the average power efficiency for high PAPR signal. The essential principle is to keep operating the PA in or close to its saturation region under various output power level. Under this principle, the power efficiency enhancement techniques usually can be classified into two categories, the supply voltage modulation and load impedance modulation.

2.1.1 Supply Voltage Modulation

In this technique, the supply voltage of the PA is modulated proportionally to the output power to keep the PA always operating in high efficiency mode. Typically, the supply voltage modulation can be separated into two types, Envelope Elimination and Restoration

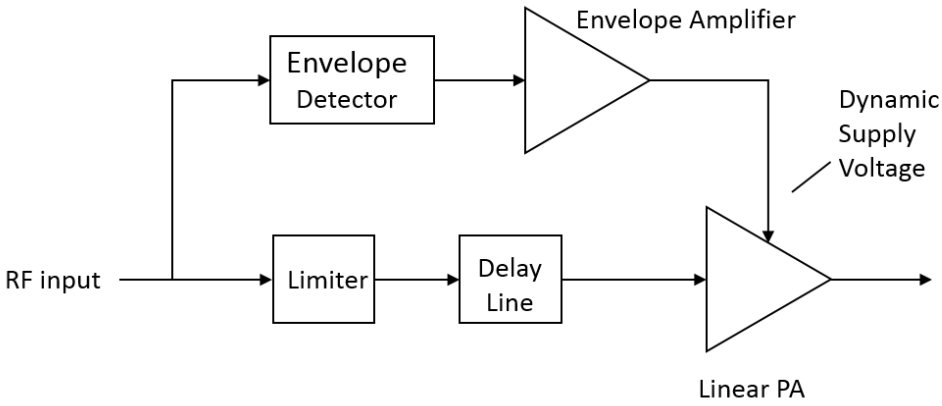

(a)

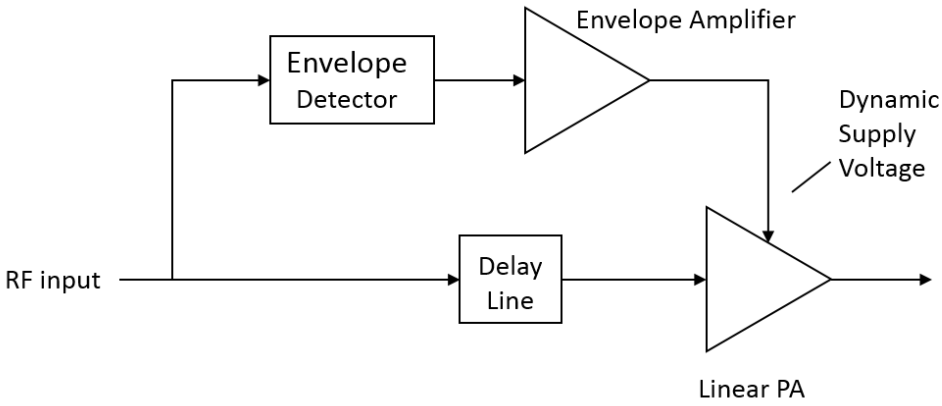

(b)

Figure 2.1: Digram of Supply Voltage Modulation.(a) EER. (b) ET

(EER) [19] or Envelope Tracking (ET) [20, 21]. Fig 2.1 shows a diagram of the two types of supply voltage modulation technique. EER relies on the integration of high efficiency switched-mode PA and envelope re-modulation techniques. On the contrary, ET uses a linear PA but with supply voltage tracking the input power. So the PA is always operating in a compression region where the power efficiency is improved. The ET technique has already been deployed to some commercial mobile devices, such as in Samsung Galaxy Note 3 and iPhone-6.

Either in EER or ET, the envelope amplifier shown in the diagram is required to be very power efficient to indeed obtain a high system efficiency. However, as the envelope signal usually spreads over a broad bandwidth, designing the envelope amplifier becomes very

hard. In addition, the envelope amplifier also needs to cover a wide dynamic range for high PAPR signal, which makes envelope amplifier design even more difficult. However, the broad bandwidth and high PAPR signal will be used in next generation of wireless communication (5G), so deployment of supply voltage modulation becomes very challenging.

2.1.2 Load Impedance Modulation

Another efficiency enhancement technique relies on a load impedance modulation mechanism. This method leverages on driving the PA always with maximum voltage swing by varying the load impedance at different power levels. Two classical examples using such techniques are Outphasing PA [22–25] and Doherty PA (DPA) [26]. Fig 2.2(a) and fig 2.2(b) show the typical diagram of the Outphasing PA and Doherty PA respectively.

Both of these two techniques employ two or more PA units to realize the impedance modulation. In Outphasing PA, two branches of PA unit are driven into saturation mode by two signals with opposite phase modulation. The load impedance modulation is implemented by combining the PA outputs. In Doherty PA, the load modulation is, however, created by asymmetric currents injection into the combining point and impedance transformation from the quarter wavelength transmission line. Recently, Doherty PA caught many attentions by PA designers as it presents potentials to meet efficiency requirement of next generation communication system.

2.1.3 Linearity Enhancement

All of the efficiency enhancement methods mention above utilize the saturation mode of transistors, so PA suffers from severe nonlinear distortions. Among the many developed linearization techniques, Digital Pre-Distortion (DPD) is usually considered as a powerful tool. However, the improvement of signal linearity in DPD depends on the complicated modeling of PA nonlinear characteristics and complex digital signal processing, which makes DPD difficult to be realized over a broad bandwidth and a real-time system. In addition, the power-hungry nonlinear signal processing of DPD also has negative effects on system power

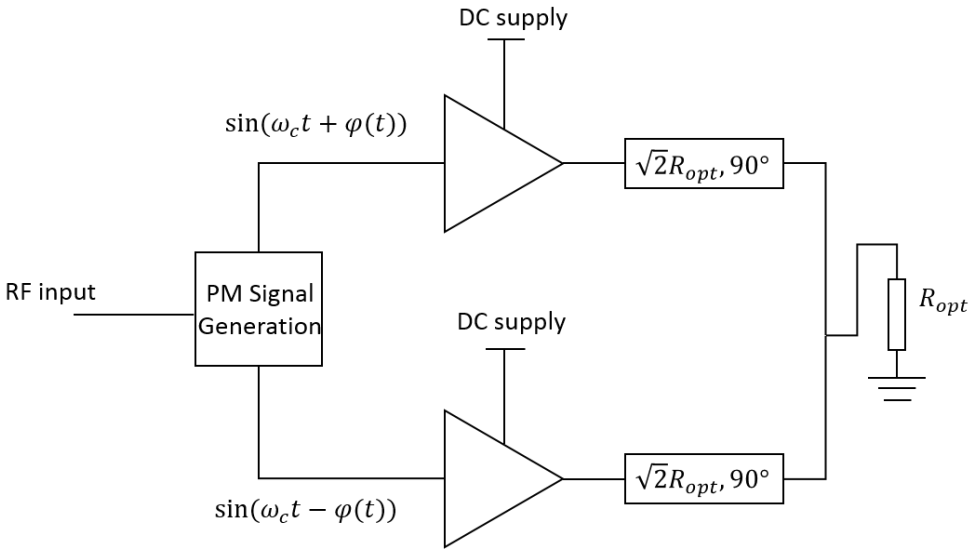

(a)

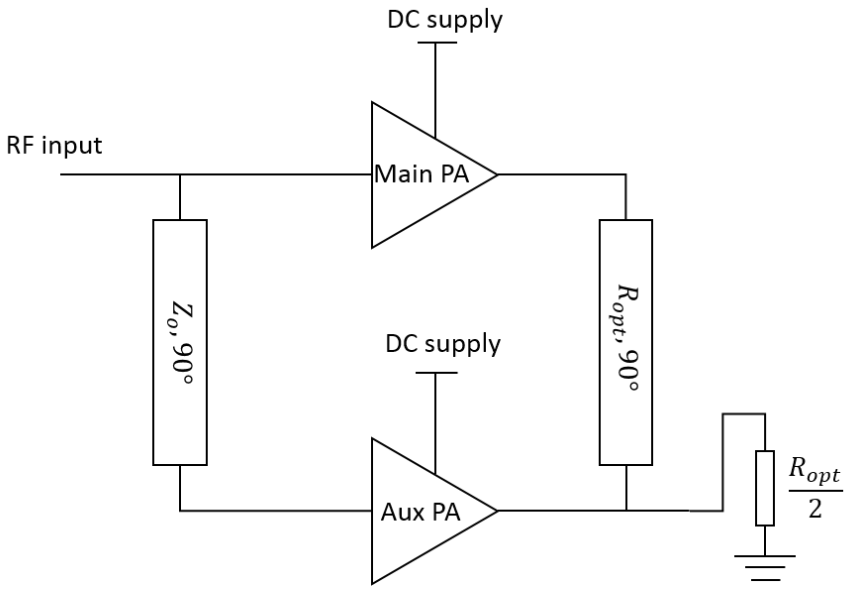

(b)

Figure 2.2: Diagram of Load Impedance Modulation.(a) Outphasing PA. (b) Doherty PA

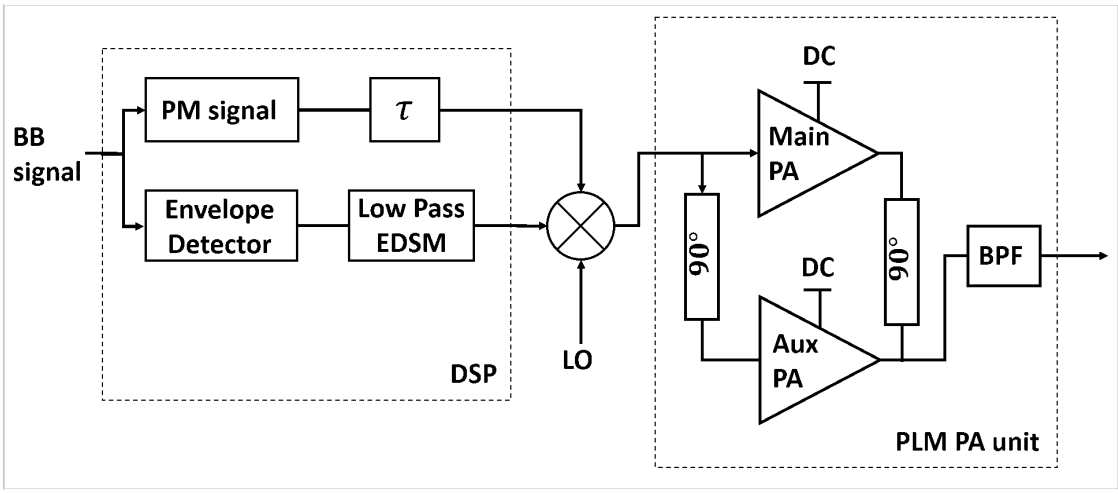

Figure 2.3: Diagram of Envelope Delta Sigma Modulation Transmitter

efficiency.

2.2 Bitstream Modulated Transmitter

Another attempt on improving power efficiency is borrowing digital PA concept. Bitstream Modulated Transmitter has been proposed under this principle. The essential idea of Bistream modulated Transmitter is to convert a non-constant envelope signal to have a "digital" fashion with bitstream type of envelope, which can be efficiently amplified by switching mode PA. Different types of bitstream modulation has been used, such as Pulse Width Modulation (PWM), Low Pass Delta Sigma Modulation (LPDSM), Envelope Delta Sigma Modulation (EDSM), etc. Among these modulations, those techniques using delta sigma modulation (DSM) utilize oversampling and noise shaping to preserve the signal fidelity by pushing the quantization noise away from the desired signal. Meanwhile, amplification of such signal by switched-mode PA provides reasonable linearity. Especially, EDSM has been proved to be suitable for RF signal because it digitizes the envelope in baseband and demands much lower sampling rate than the other DSM scheme.

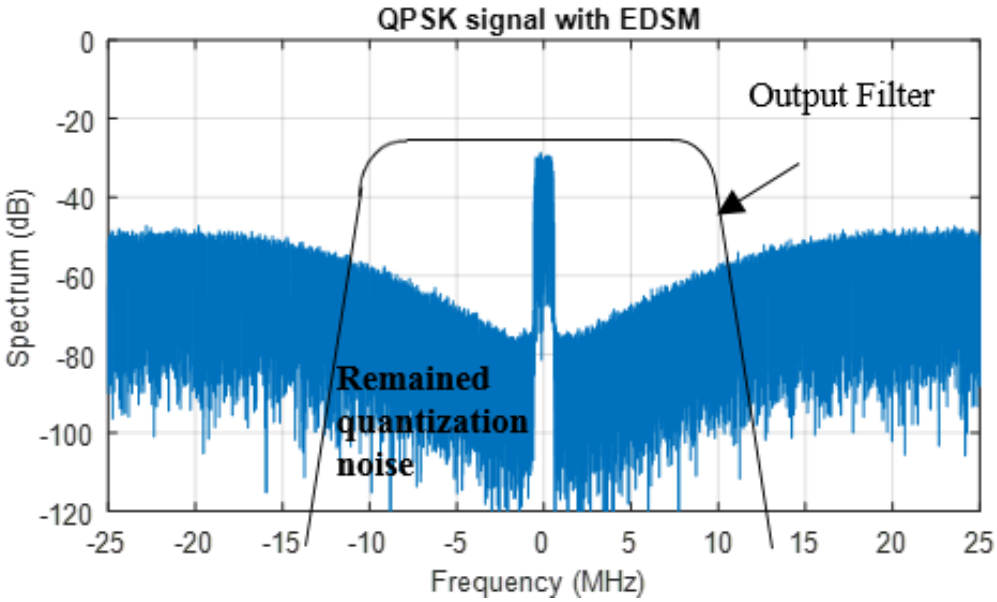

Figure 2.4: Spectrum of EDSM signal

2.2.1 EDSM transmitter

Fig 2.3 shows the diagram of EDSM transmitter. In the EDSM transmitter, the original baseband signal is split into envelope path and phase path. The envelope passes through a low pass delta sigma modulator and becomes a bitstream. Then the phase path and envelope path are reunited and up-converted to RF frequency, then amplified by PAs. The original signal is recovered by placing an band pass filter (BPF) at the output of the PA.

Fig 2.4 Shows the example of simulated EDSM signal spectrum. The test signal is 1 MSps QPSK signal with its pulse shaped by a square root raised cosine filter. The roll off factor is 0.2 so the bandwidth of the original QPSK is 1.2 MHz. 1-bit delta sigma modulation is applied and the sampling rate used in this simulation is 100 MSps. As shown in the figure, the original signal is preserved as the quantization nearby is suppressed by the noise shaping function, while the noise increases gradually as the frequency offset further from the center.

The 1-bit digitized envelope drives the the PA in a high efficiency switching mode, i.e, either in saturation region or in pinched-off region. After amplification, the original signal is restored by filtering out the quantization noise by an output filter, as shown in Fig. 2.4.

2.2.2 Pulsed Load Modulation

However, driving the PA into switching mode does not promise a high system power efficiency unless the following conditions are meet. First, the output filter must present low insertion loss to avoid wasting in band signal power. Second, as the quantization noise power is usually not negligible or even comparable to the desired signal power, it must be reflected and recycled to preserve the system power efficiency. To achieve this goal, the system need two conditions. First, the PA should perform as a voltage source. Second, the output filter needs a high quality factor Q and behaves as current rejection filter at its stopband.

In conventional switched-mode PA schemes, Class-D PA with DSM meets this requirement. Ideally, Class-D PA can obtain 100% power efficiency. But the parasitic capacitance on the transistors limits its operating frequency and it is not suitable for high frequency application. Pulsed Load Modulation (PLM) [8] PA was proposed to solve this problem by emulating a RF switching voltage source. Fig 2.5 shows the diagram of PLM PA units.

Similar to a Doherty PA, the PLM unit combines two sets of PA by a quarter wavelength transmission line. Different from the asymmetric biasing in Doherty, the main PA and auxiliary PA in PLM are biasing at similar condition, such as Class-B mode, and switching between pinch-off and saturation mode simultaneously if driven by 1-bit EDSM signal. When both of the PAs are turned on, the PLM unit outputs maximum voltage swing and the auxiliary PA presents low impedance to the combining junction. When the two PAs are switched off, the main PA output an open circuit or high impedance, which is later transformed to short circuit or low impedance at the junction. Therefore, a RF switching voltage source is formed. Once the output filter performs as a current rejection mode in its stopband, the quantization noise is equivalently reflected back to the PA and recycled to power supply. So the original signal can be recovered without degrading the system efficiency.

The PLM units and the high Q filter impose a RF switching resonator [27] whose impedance is modulated by the duty cycle of the pulses driving it. Let the duty cycle of the input pulses be denoted by D, and the maximum voltage swing and maximum output current as V_{max} and I_{max} respectively. The load impedance seeing from the junction point

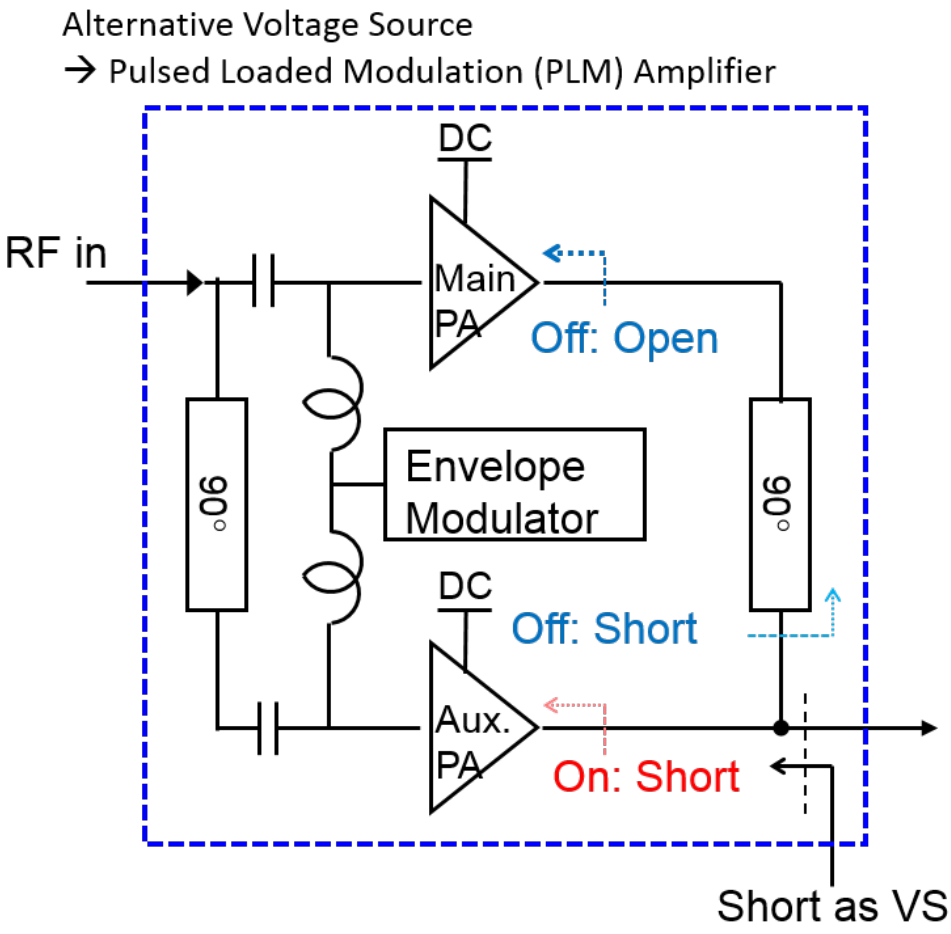

Figure 2.5: Diagram of Pulsed Load Modulation PA

is expressed as: [8]:

$$R_{eff} = \frac{V_{max}}{I_{out}} = \frac{1}{D} \cdot R_{opt}/2 \tag{2.1}$$

with output power of:

$$P_{out} = \frac{1}{2} V_{max} I_{max} D^2 \tag{2.2}$$

Note that the output power is proportional to square of the duty cycle D. The load impedance to the main PA and auxiliary PA can be expressed as:

$$R_{main} = \begin{cases} R_{opt} & D > 0.5 \\ 2 - D \cdot R_{opt} & 0 < D < 0.5 \end{cases} \tag{2.3}$$

$$R_{aux} = \begin{cases} \dfrac{1}{1-D} \cdot R_{opt} & D > 0.5 \\ \infty & 0 < D < 0.5 \end{cases} \tag{2.4}$$

When the duty cycle is larger than 50%, the main PA is terminated with optimum efficiency and the auxiliary PA is operating in saturation mode, so a flat maximum efficiency can be obtained. When the duty cycle is smaller than half, or the output power back off beyond 6 dB, the efficiency decreases as the load impedance to main PA drops proportionally to the D. Then the PLM unit shows the same efficiency as a class B PA. A typical PLM PA efficiency performance is plotted in Fig 2.6 [8].

2.3 Noise Suppression

In previous EDSM transmitter, the signal envelope is digitized to a 1-bit sequence. The restoration of the original signal in EDSM transmitter relies on the noise shaping of DSM and the output BPF. However, the 1-bit EDSM with limited sampling rate may create strong quantization noise within the filter passband. To sufficiently suppress the quantization noise, intuitively people may consider the following methods: first, increasing the oversampling ratio or using higher order DSM; second, employing a narrow band BPF. Unfortunately, higher oversampling ratio often increases the system cost and the required sampling frequency may not even be feasible, especially for broadband signal. However, the low loss and narrow

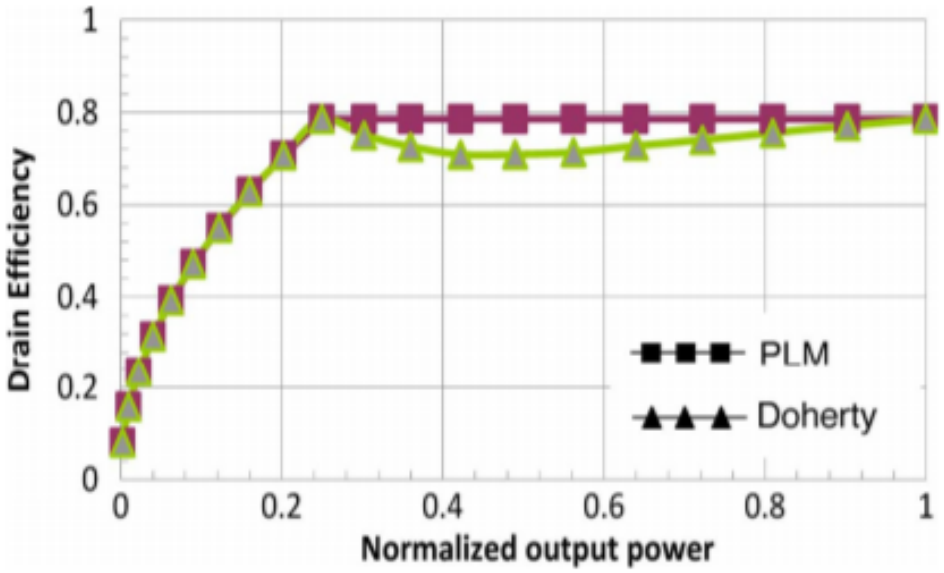

Figure 2.6: Efficiency of PLM PA

band BPF leads to a very high quality factor, which is difficult to be achieved at high frequency.

In previous research, two additional noise suppression methods have been proposed. The first one is the multi-level EDSM, which quantizes the signal envelope to more than two levels so the quantization noise level is reduced. The second method introduces an active noise filtering by emulating a digital FIR filter scheme at RF.

2.3.1 Multi-level EDSM

Rather than converting the non-constant envelope to either 0 or 1(maximum), the multi-level EDSM uses a multi-level digitizer in the DSM chain so the quantization noise level is intrinsically smaller. Fig 2.7 [9] shows the simulated spectrum of 5 MHz WCDMA signal with different level EDSM. The sampling rate is 2 GSps. From the spectrum plot, the 3-level EDSM has much lower quantization noise than 2-level case.

In 1-bit or 2-level EDSM, the PA is switching between pinch-off or saturation mode so the optimal efficiency can always be obtained. But in multi-level cases, the intermediate

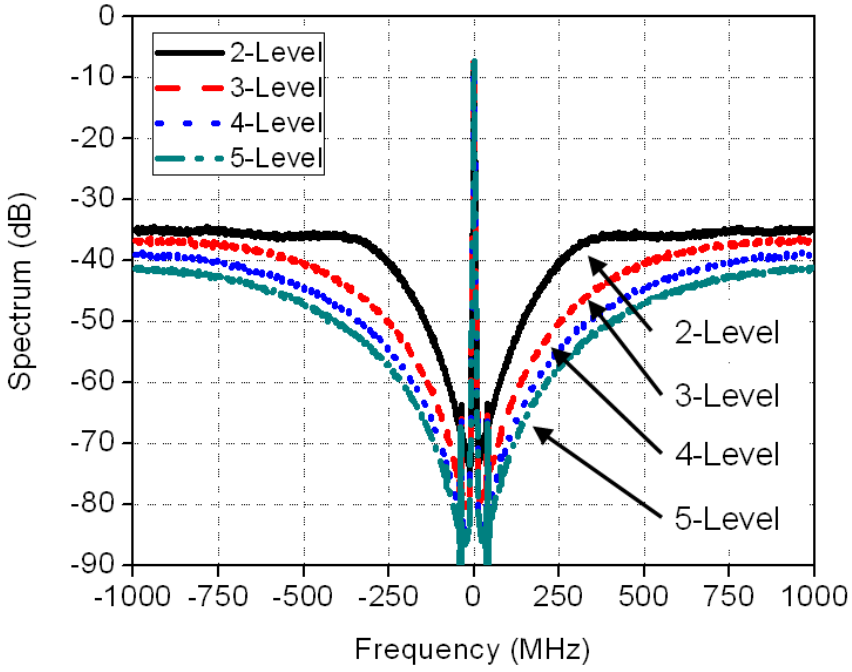

Figure 2.7: Simulated spectrum of 5 MHz WCDMA signal with different level EDSM [9]

output power levels lead to poorer efficiency. So the average power efficiency trends to be lower than the 2-level case. However, as the quantization noise level is reduced, the in band signal occupies more portion of total power. So after filtering out the noise, the effective power efficiency of the desired signal might be higher with some quantization levels.

However, as shown in Fig. 2.7, the improvement on the quantization noise is less significant when the quantization level beyond 3. In addition, the noise reduction by finite level EDSM is limited with fixed sampling frequency. So further noise suppression method is demanded.

2.3.2 Active Noise Filtering

Alternatively, people propose an active noise filtering scheme as a complementary noise suppression method to an analogue filter. It leverages on a delaying and combining structure of multiple power amplifiers to create an Finite Impulse Response (FIR) filter in an analogue

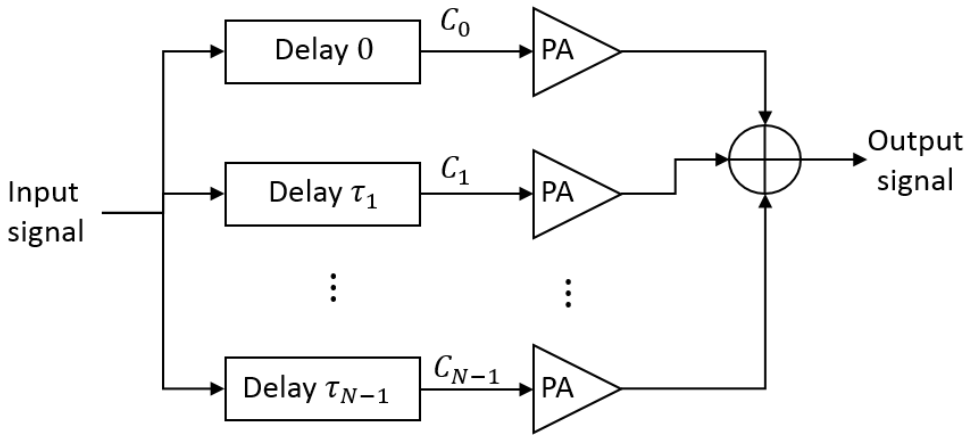

Figure 2.8: Diagram of Active FIR filter

fashion. Fig 2.8 displays the principle of this method. The input signal is directly split into different delay lines, and amplified, then recombined. Let the input signal be denoted by $x(t)$, then for the n^{th} branch, the delayed version of the input with combining coefficient is $C_n x(t-\tau_n)$. In the bitstream modulated transmitter, as a digitized envelope signal is amplified by a switching mode PA, the nonlinear distortion from the PA is less significant than the quantization noise. Assume all the PAs have same gain of A, the output of n^{th} channel can be approximately written as $AC_n x(t-\tau_n)$. So the combiner output will be:

$$y(t) = \sum_{n=0}^{N-1} AC_n x(t-\tau_n) \tag{2.5}$$

Which has a spectrum expression of:

$$Y(f) = AH(f) \cdot X(f) \tag{2.6}$$

where $H(f)$ is the frequency response of the equivalent FIR filter

$$H(f) = \sum_{n=0}^{N-1} C_n e^{-j2\pi\tau_n f} \tag{2.7}$$

The delay operation in the time domain leads phase differences between each branch in frequency domain. When all the branches are combined in phase, they form passband; when the signals are added out of phase, they create a null or a rejection band. The filter characteristics, such as bandwidth and passband location, are determined by the delay lines

and the combining coefficients. With different combining coefficient, one can obtain different types of filter. For example, for a N-channel uniform combining case, let the time delay increment be t_0 and combining coefficient be 1, the filter frequency response is:

$$\begin{aligned} H_{uniform}(f) &= 1 + e^{-j2\pi t_0 f} + e^{-2\cdot j2\pi t_0 f} + \cdots + e^{-(N-1)\cdot j2\pi t_0 f} \\ &= \frac{1 - e^{-N\cdot 2\pi t_0 f}}{1 - e^{-j2\pi t_0 f}} \end{aligned} \tag{2.8}$$

Or if binomial combining coefficient is applied, i.e, $C_n = \binom{N}{n}$, the filter response becomes:

$$\begin{aligned} H_{binomial}(f) &= 1 + \binom{N}{1} e^{-j2\pi t_0 f} + \binom{N}{2} e^{-2\cdot j2\pi t_0 f} + \cdots + e^{-(N-1)\cdot j2\pi t_0 f} \\ &= (1 + e^{-j2\pi t_0 f})^N \end{aligned} \tag{2.9}$$

Fig 2.9 shows a plotted frequency response of these filters with N = 4. Note that the filter has multiple passbands and rejection bands because of the periodically changing phase differences. If all the combining coefficents are postive real numbers, the first passband provides a low pass behavior, while the higher order passband gives a bandpass filter. For EDSM transmitter, the bandpass characteristics can be used to suppress the quantization noise at RF. In the work done by Y.Song, et al [15], a X-band EDSM transmitter with two channels active noise filtering is proposed, in which the time delay is produced by a transmission line. It is important to notice that both the bandwidth and location of the higher order passband are inversely proportional to delay length. Therefore, longer delay line is required to achieve narrower band filter. However, once the bandwidth is selected, the position of each the higher order passband is also determined. This implies the BPF mode of the active filter has limited flexibility of choosing bandwidth and passband frequency. In addition, the center frequency of the higher order passband becomes more sensitive to delay errors as the order increases, so the delay operation must be precise enough. One way to compensate such defect is using a phase shifter to tune the phase difference between each channel and forces them to be combined in phase at desired frequency [15]. But the insertion loss from the long delay line and phase shifter causes unwanted power dissipation and degrades overall efficiency. Furthermore, the filter bandwidth is still not tunable with fixed delay lines.

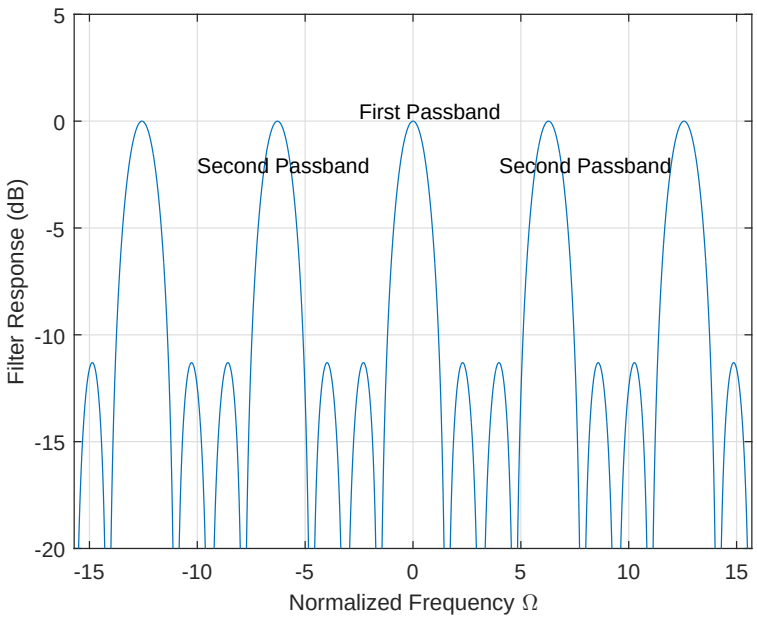

(a)

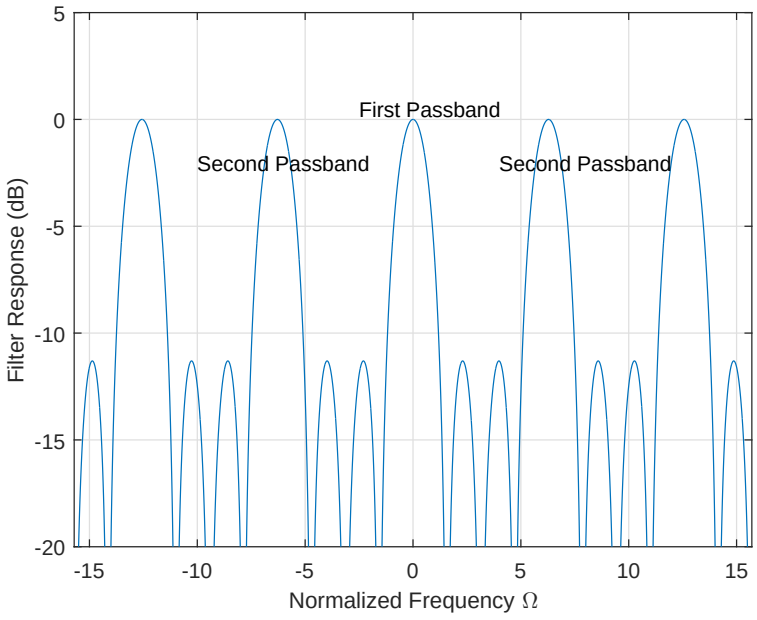

(b)

Figure 2.9: Frequency Response of Active FIR filter. (a) Uniform Combining.(b) Binomial Combining

CHAPTER 3

Channelized Active Noise Elimination

3.1 Principle

To overcome the issues in the BPF mode of the active FIR filter, we propose an alternative active noise filtering techniques called channelized active noise elimination (CANE). Rather than directly use the higher order passband of the FIR structure, CANE uses the up-converted version of the low pass characteristic to form a band pass filter. Therefore, the center frequency of passband is decoupled with the delay operations. Fig 3.1 shows the diagram of the CANE technique.

The original baseband signal is firstly converted to a bitstream envelope style by a low pass EDSM processor, then split into multiple channels of baseband delay lines. Then these delayed signals are up-converted to the same RF carriers, amplified by a set of identical PAs, and recombined by a RF power combiner. By doing so, the filter characteristics of the active FIR is up-converted to RF as well as the baseband signal. Then the first passband or the low pass filter profile becomes a BPF. As shown in fig 3.1, let the baseband EDSM signal be denoted by $x(t)$, the delayed version of input in the n^{th} channel is $C_n x(t-\tau_n)$. Here C_n is the combining coefficient. After up-converted to carrier $e^{2\pi f_c t}$, the RF input to the PA in n^{th} channel is

$$x'(t) = C_n x(t-\tau_n) \cdot e^{2\pi f_c t} \tag{3.1}$$

Since the PAs are identical to the each other, they share the same power gain A. Also, the quantization noise is the dominant unwanted distortions. Therefore, the output signal from the power combiner can be approximately expressed as:

$$y(t) = Ae^{2\pi f_c t} \sum_{n=0}^{N-1} C_n x(t - \tau_n) \tag{3.2}$$

In frequency domain, the spectrum of the output signal is then:

$$\begin{aligned} Y(f) &= AH_B(f - f_c)X(f - f_c) \\ &= AH(f)X(f - f_c) \end{aligned} \tag{3.3}$$

Here, $H_B(f)$ is the equivalent frequency response of the baseband active FIR filter, as given by equation (2.7). For simplicity, let the all of combining coefficient C_n be positive real number, then the first passband in $H_B(f)$ exhibits a low pass filter profile as all the channels are added in phase at $f = 0$. $H(f)$ represents the frequency response of the CANE filter, which is same as $H_B(f)$ except its center frequency is shifted to f_c. This means that $H(f)$ holds a passband centered at f_c, so a BPF profile is formed.

The characteristics of this BPF, such as filter shape and bandwidth, are determined by the time delay and combining coefficients. However, the center frequency of the main passband is controlled by the LO frequency and irrelevant to the delay length. Therefore, the position of BPF on frequency axis is no longer sensitive to the delay errors. In addition, the filter can change the delay length to create arbitrary bandwidth without disturbing its center frequency.

For example, in a N-channels uniform combining case, let the combining coefficient be $C_n = 1, for\ n = 0, 1, 2, ..., N - 1$, and the delay increment step be t_0. Then the time delay in n^{th} channel is $n \cdot t_0$, so the equivalent filter response is :

$$\begin{aligned} H(f) = H_B(f - f_c) &= \sum_{n=0}^{N-1} e^{-n \cdot j2\pi t_0 (f - f_c)} \\ &= \frac{sin(N\pi t_0(f - f_c))}{sin(\pi t_0(f - f_c))} \cdot e^{-j(N-1)\pi t_0 (f - f_c)} \end{aligned} \tag{3.4}$$

At the center frequency, $|H(f)|$ reaches its maximum value and forms a passband,

$$H(f_c) = N = max\{|H(f)|\} \tag{3.5}$$

When $|H(f)| = 0$, the nulls of $H(f)$ exist and produce the rejection bands. The positions

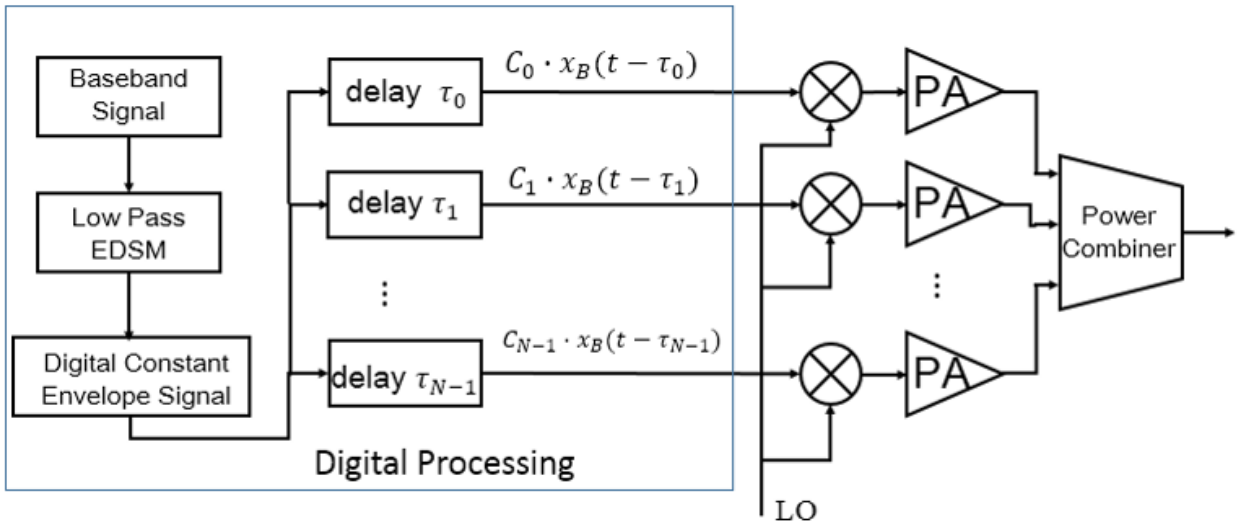

Figure 3.1: Diagram of Channelized Active Noise Elimination

of the nulls are given by:

$$f_{rej} = f_c \pm \frac{M}{Nt_0} \tag{3.6}$$

where M is an integer and $M \neq kN, k = 0, 1, 2, 3, ...$ The null to null bandwidth of this BPF is given by

$$BW_{null} = \frac{2}{Nt_0} \tag{3.7}$$

Note that the positions of higher order passbands are also shifted by f_c on frequency axis. So these passbands locate at:

$$f = f_c \pm \frac{k}{t_0}, k = 0, 1, 2, ... \tag{3.8}$$

Compare (3.6) and (3.8), it can be observed that (N-1) nulls are placed between the main passband and its adjacent passband, which creates a flatter and wider stopband. So with more channels, the CANE filter usually provides better noise suppression.

3.2 Noise Suppression with CANE

3.2.1 Simulation of EDSM with CANE

To validate the noise suppression ability of CANE in a EDSM transmitter, we first simulate the spectrum of the equivalent baseband signal system output. Fig 3.2 shows the simulated spectrum. The test signal used here is 1MSps QPSK signal whose pulses are shaped by square root raised cosine filter with roll-off factor of 0.2. So the in band signal occupies 1.2MHz bandwidth. The 2-level EDSM is employed to digitize the envelope. The sampling rate and resolution bandwidth used in this simulation are 100MSps and 50KHz respectively. The blue curves in these plots show the spectrum of original EDSM before active noise filtering. The red curves then show the noise suppression from different CANE filters.

Fig 3.2(a) displays a 2-channel CANE filter with time delay $t_0 = 50nS$. Clearly a filter response can be observed. The first pair of nulls locate at 10 MHz offset from the center frequency, which is agreed with equation (3.6). The quantization noise near the in band signal is reduced in these two rejection bands. Also, it can be seen that both the passbands and rejection bands show up repeatedly with period of 20 MHz. In Fig 3.2(b), the delay length is extended to 100 nS. Then the first pair of nulls pull back to 5 MHz away from the center and the filter bandwidth shrinks to the half. Meanwhile, the higher order passbands and rejection bands also repeat more frequently. Generally, with same number of channels and combining coefficients, longer delay length leads to a narrower bandwidth, as predicted by equation (3.7).

Fig 3.3(c) shows a 4-channel uniform combining case whose delay increment step is 30 nS. Because of its wider rejection band, the 4-channel CANE filter provides better noise suppression than 2-channel cases. Fig 3.3(d) presents a 4-channel binomial combining CANE filter with same time delay. Considering the noise suppression near the desired signal, the binomial combining shows better results than the uniform combining case.

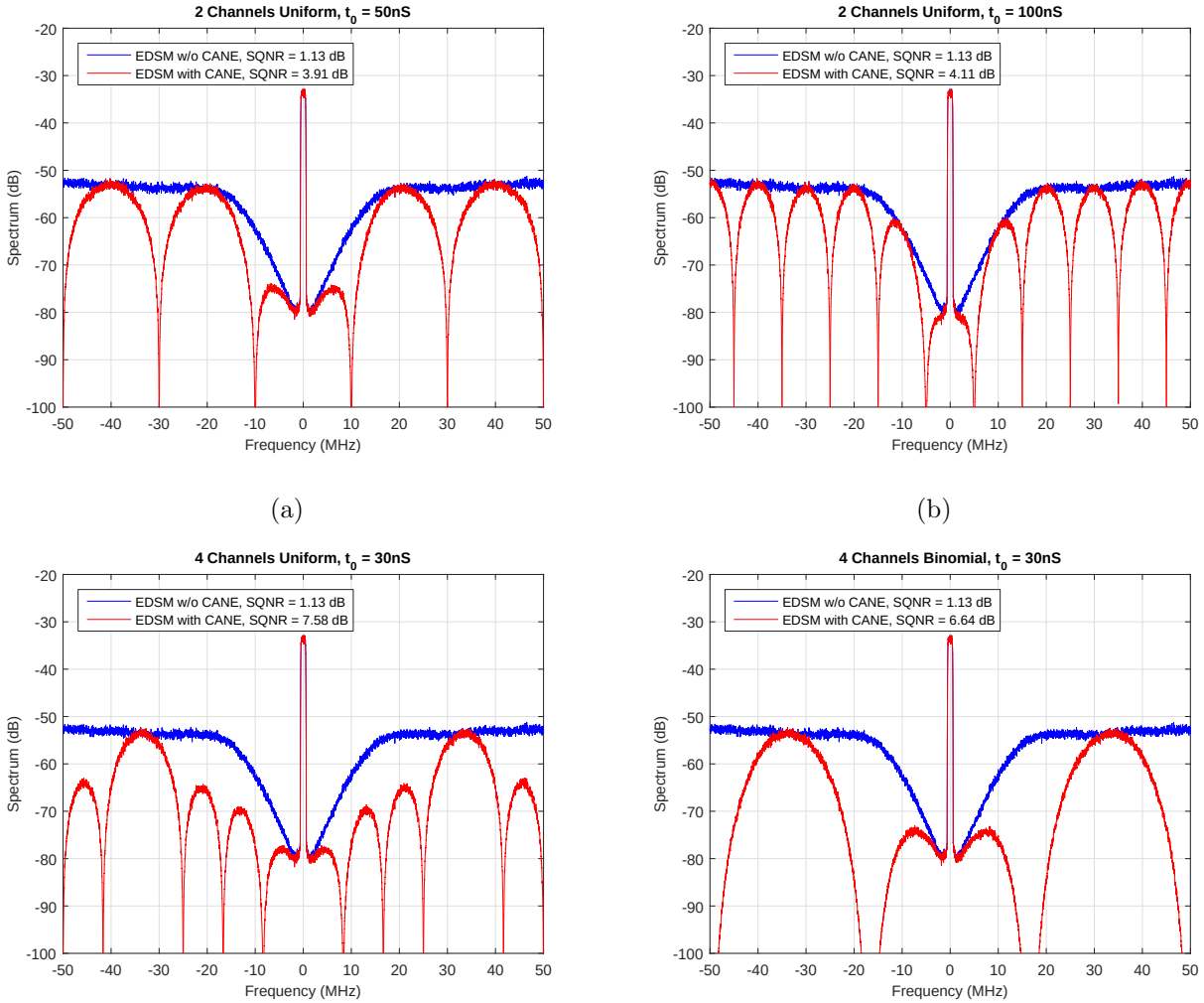

Figure 3.2: Simulated Spectrum of 2 level EDSM with CANE. The blue cures shows the spectrum of original EDSM signal without any active noise filtering. The red curves displays the spectrum of EDSM with different types of CANE filter. (a) 2-channel combining with delay step=50 nS. (b) 2-channel combining with delay step = 100nS. (c) 4-channel uniform combining with delay step=30 nS. (d) 4-channel binomial combining with delay step=30 nS.

3.2.2 Signal to Quntization Noise Ratio

The active noise filtering can be intuitively observed from the spectrum plots. But to quantify the noise suppression performance, the signal to quantization noise ratio (SQNR) and in band signal power occupation should be considered. The definition of the SQNR is the ratio of the in band signal power over the out of band quantization noise power.

$$SQNR = \frac{P_{sig}}{P_{QN}} \tag{3.9}$$

P_{sig} is the in band signal power, which can be calculated by:

$$P_{sig} = \int_{-sig\_bw/2}^{+sig\_bw/2} S_{bb}(f)df \tag{3.10}$$

where S_{bb} represents the power spectrum density of equivalent baseband of the system output, and sig_bw is the bandwidth of desired signal. The out of band quantization noise power P_{QN} can be calculated by:

$$P_{QN} = \int_{-F_s/2}^{-sig\_bw/2} S_{bb}(f)df + \int_{+sig\_bw/2}^{+F_s/2} S_{bb}(f)df \tag{3.11}$$

where F_s is the sampling frequency of the EDSM.

Because the noise shaping function in DSM pushes the quantization noise to higher frequency, the in band signal power can be regarded as the desired signal power and the out of band noise power approximately represents the total noise strength. So the ratio of the two offers an index for evaluating the signal fidelity in this system.

The simulated SQNR of each case is listed in Fig 3.2. Without any active noise filtering, the EDSM signal has SQNR of 1.13 dB. For 2-channel CANE, the SQNR is increased to 3.91 dB and 4.11 dB with delay of 50 nS and 100 nS respectively. In 4-channel uniform combining, the SQNR then is improved by 6.45 dB with delay step of 30 nS. With same delay length, the 4-channel binomial combining improves SQNR by 5.51 dB. Typically, 2-channel combining can improve the SQNR by about 3 dB, which means that the quantization noise power is approximately reduced by half. While in the 4-channel uniform combining, two additional channels introduce one more bit of the envelope resolution of the combined signal, so another approximate 3 dB improvement on SQNR is observed.

	SQNR	Signal Power (%)	SQNRF	Signal Power in Filter (%)
EDSM w/o CANE	1.13	56.46%	14.05	96.21%
2-ch, $t_0 = 50nS$	3.91	71.09%	20.40	99.1%
2-ch, $t_0 = 100nS$	4.11	72.03%	17.98	98.43%
4-ch/uniform $t_0 = 30nS$	7.58	85.14%	26.53	99.78%
4-ch/binomial $t_0 = 30nS$	6.64	82.18%	29.07	99.88%

Table 3.1: SQNR and In band signal power in 1-bit EDSM with or without CANE

According to the chart, more channels usually offer better noise suppression. But in some cases when the number of PA channels is limited, a combo of CANE and multi-level EDSM can be used to achieve better SQNR. Fig 3.3 shows the simulated spectrum of CANE with 3-level EDSM.

One interesting observation is that the 2-level EDSM with 2-channel CANE has similar improvement on SQNR as 3-level EDSM without noise filtering. In fact, both of the two cases share the same "1.5 bit" envelope resolution, which means that their quantization noise power might be similar.

Note that CANE technique often cooperates with an output BPF, so it is important to evaluate the SQNR within the analogue filter passband. For simplicity, we assume an ideal BPF is placed at the power combiner output, then a signal to quantization noise ratio with filter (SQNRF) can be defined as:

$$\begin{aligned} SQNRF &= \left.\frac{P_{sig}}{P_{QN}}\right|_{withinFilter} \\ &= \frac{\int_{-sig\_bw/2}^{+sig\_bw/2} S_{bb}(f)df}{\int_{-FBW/2}^{-sig\_bw/2} S_{bb}(f)df + \int_{+sig\_bw/2}^{+FBW/2} S_{bb}(f)df} \end{aligned} \tag{3.12}$$

For example, we can calculate the SQNRF by assuming a BPF with 30MHz bandwidth being applied to the signals shown in Fig 3.3. The modified SQNRs are listed in Table 3.1.

The higher SQNR not only means less noise, but also reflects that the in band signal occupies more power in the total spectrum. In other words, the effective power efficiency of

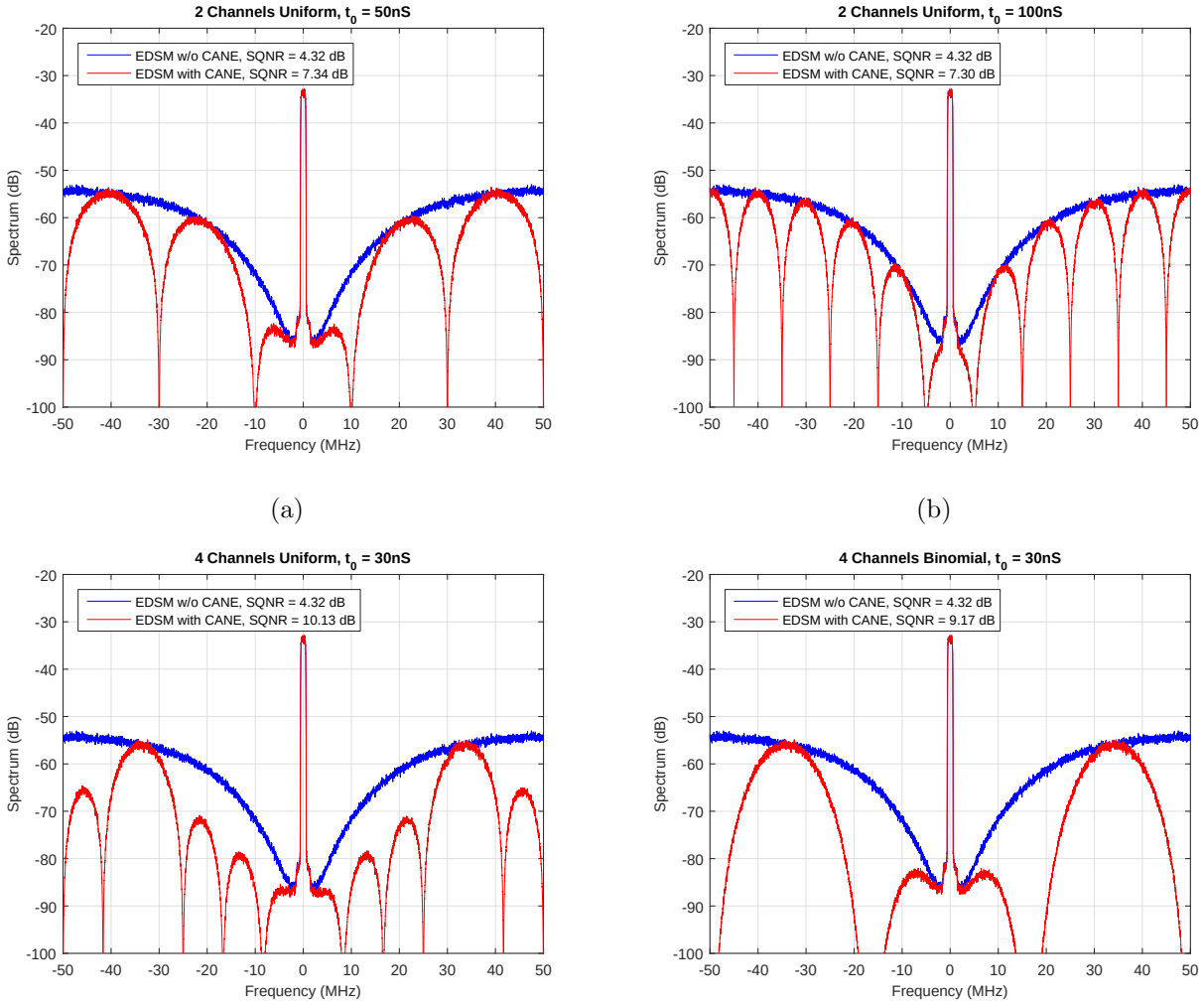

Figure 3.3: Simulated Spectrum of 3 level EDSM with CANE. The blue cures shows the spectrum of original EDSM signal without any active noise filtering. The red curves displays the spectrum of EDSM with different types of CANE filter. (a) 2-channel combining with delay step=50 nS. (b) 2-channel combining with delay step = 100nS. (c) 4-channel uniform combining with delay step=30 nS. (d) 4-channel binomial combining with delay step=30 nS.

the desired signal becomes higher. Table 3.1 also lists the percentages of the in band signal power over the entire signal and within the ideal analogue filter. From the chart, we can observe that every single dB improvement on SQNR results in better effective efficiency. With four channels combined together, the noise residual is less than 1% in the filter, which means little output power is wasted on the noise. However, the calculated SQNRF and percentage of in band signal within the BPF overestimate the noise suppression performance in real application, because the actual analogue filter cannot offer a perfect bandpass response.

3.3 Digital control and calibration

As shown in Fig 3.1, CANE creates time delay before up-converting the signals, so the delaying operation can be directly implemented through baseband digital signal processing without using any physical delay structure. On the other hand, the decoupling of center frequency and bandwidth of the CANE filter enables a software controlled re-configurable filter. By programming the delay length, CANE can achieve arbitrary filter bandwidth without changing any hardware. Meanwhile, as all the channels share identical baseband signal, the digital delay can be easily generated by shifting the data points in the DSP memory, as shown in Fig 3.4. To change the delay length, one only needs to shift the data-read-pointer to a different memory address. Therefore, CANE produces a real-time tunable filter.

Another benefit from the baseband signal processing is that CANE is robust to hardware deviations. Previous analysis assumes all the RF channels are identical to each other. But in reality, it is reasonable to expect more or less phase and amplitude variations between each RF circuit. Since all the channels share the same analogue circuits topology, one way to minimize the errors is using a consistent fabrication technique. However, CANE can easily calibrate the deviations in the analogue parts by pre-shifting the phase and equalizing the amplitude of the complex baseband signal.

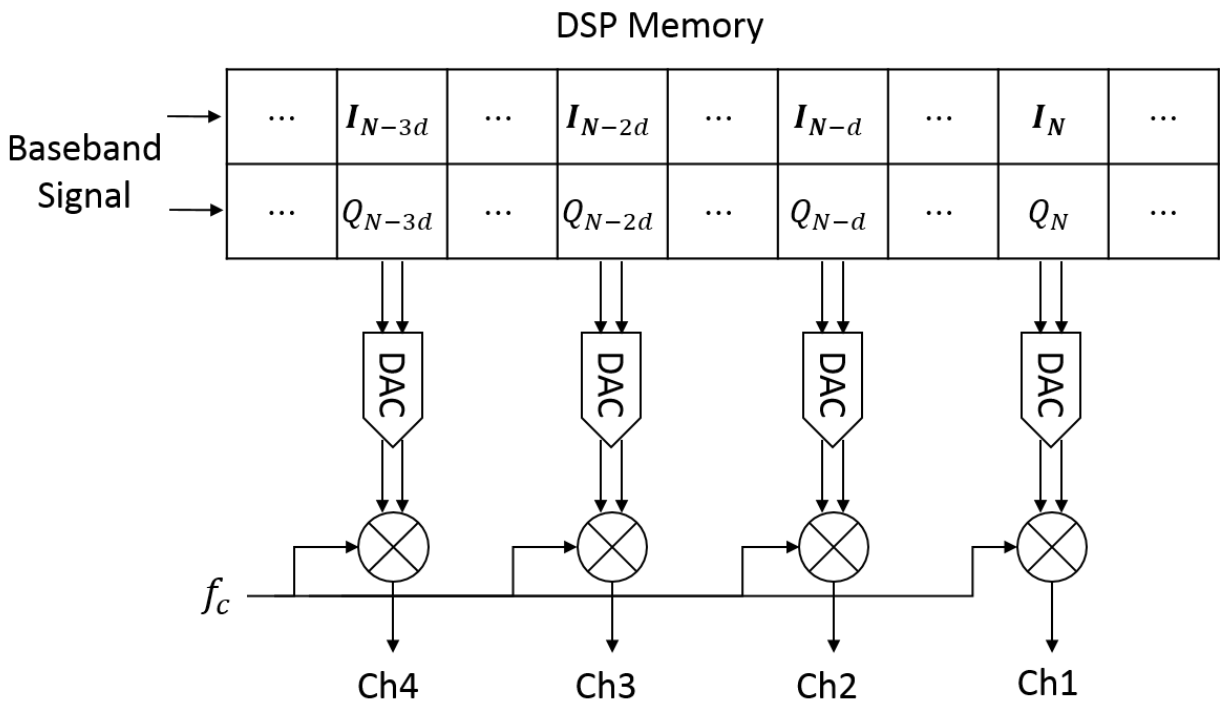

Figure 3.4: Implementation of digital baseband delay lines

3.4 Power efficiency preservation

3.4.1 Power Combining in Active Noise Filtering

In previous section, the CANE filter is discussed in system level. But in the power amplifiers, the power efficiency must be preserved while suppressing the quantization noise. As shown in previous section, the quantization noise occupies about half of the output power if not being suppressed. So if the noise power is not rejected in a power saving mode, the system power efficiency will be significantly reduced. In conventional EDSM transmitter, the Pulsed Load Modulation PA operates as a RF switching voltage source and the output cavity filter serves in current rejection mode in the stopband. The pair of the PLM PA and the filter actually forms a load impedance modulation in frequency domain. For the in band signal, the filter terminates the PA by matched load impedance. But for the out of band noise, the filter presents open circuit or high impedance so that the noise power is reflected to the PA and equivalently recycled to power supply.

As CANE relies on the combining of multiple channels, the similar frequency domain load modulation can be achieved by the power combining operation. First of all, lossy power combiner might not be used in CANE because the rejected noise power will be absorbed by the lossy component, such as the cross resistor in Wilkinson combiner. Lossless power combiner is preferred but it must satisfy the following two conditions. First, the power combiner should present the optimum load impedance for in band signal and combine all the channels constructively with low insertion loss. Second, it should terminate the PA with high impedance when the quantization noise are combined out of phase.

The optimum matched load in the passband can be easily obtained by using a symmetric combiner topology as the PAs are intrinsically isolated to each other if combined in phase. Various designs of such combiners have been developed, while the major concern is minimizing the insertion loss.

The second condition, however, requires special deign of the power combiner. The active FIR filter has periodical nulls in its frequency response, where all the channels are canceled by each other. Around these nulls, the noise power is better suppressed than at the other frequencies. Therefore, as the rule of thumb, recycling the noise power around these nulls is most critical. Typically, the out of phase combining of the PAs generates a virtual ground at the combiner junctions. For example, in the case of two channels uniform combining using symmetric T-junction based combiner, the 180 degree phase different of the two PA forms an odd mode and thus the combining point presents a virtual short circuit. However, if a quarter wavelength transmission line is inserted between the combining point and each PA output, the virtual short circuit is then transformed to open circuit looking out from the PAs. This implies that the Chireix combiner, as show in Fig 3.5, can be a good candidate for 2-channel CANE. Also, similar principle can be used to guide the design of power combiner for mulit-channel combining cases.

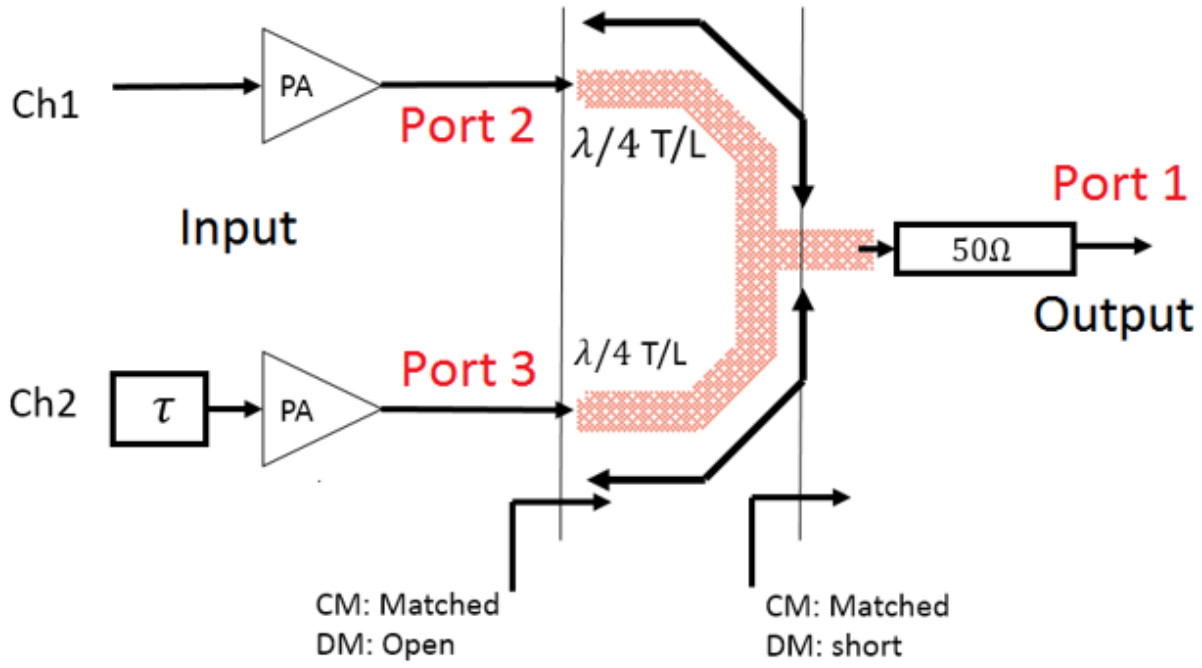

Figure 3.5: Chireix Combiner with frequency domain Impedance modulation

3.4.2 2-channel combiner Design

As mentioned in previous section, the 2-channel CANE can utilize Chireix power combiner. Different from Wilkinson combiner, Chireix type combiner is a lossless three port device whose ports are not isolated. Therefore, the input impedance looking into the each port depends on the network excitation. For example, the S parameter of this Cheirix combiner is

$$[S] = \begin{bmatrix} 0 & -j/\sqrt{2} & -j/\sqrt{2} \\ -j/\sqrt{2} & 1/2 & -1/2 \\ -j/\sqrt{2} & -1/2 & 1/2 \end{bmatrix} \tag{3.13}$$

The ports are defined as: port 1 is the combiner output, port 2 and port 3 are two inputs. To analysis the impedance modulation function,, let the excitation signal be $[V^+] = [0, V_2^+, V_3^+]^T$. Because the PLM PA used in CANE emulates switching voltage source, the two input ports are excited by maximum voltage swing but with different phase, i.e, $V_2^+ = V_0$

and $V_3^+ = V_0 e^{j\theta}$. Then the outgoing signal is given by

$$[V^-] = [S][V^+] \tag{3.14}$$

For the in band signal, port 2 and port 3 inject same signal into the network, which excite an even mode. let $V_2^+ = V_3^+ = V_0$ then $[V_+] = [0, V_0, V_0]$. The outgoing wave is then:

$$[V^-] = [-j\sqrt{2}V_0, 0, 0]^T \tag{3.15}$$

From equation (3.15), port 2 and port 3 are seeing matched load as no signal reflected back.

On the contrary, in the filter rejection band, the two inputs signal has 180 degree phase difference, so $V_2^+ = -V_3^+ = V_0$. Thus the combiner is operating in odd mode. Using equation (3.14), the out going wave is then:

$$[V^+] = [0, V_0, -V_0]^T \tag{3.16}$$

Then the equivalent reflection coefficients of port 2 and port 3 are:

$$\Gamma_2 = \frac{V_2^-}{V_2^+} = \frac{V_0}{V_0} = 1 \tag{3.17}$$

$$\Gamma_3 = \frac{V_3^-}{V_3^+} = \frac{-V_0}{-V_0} = 1 \tag{3.18}$$

So the equivalent input impedance at these two ports are:

$$Z_{2,3} = Z_0 \frac{1 + \Gamma_{2,3}}{1 - \Gamma_{2,3}} = \infty \tag{3.19}$$

Therefore, the two ports are indeed presenting open circuit to the PA output.

3.4.3 4-channel combiner Design

The design of 2-channel combiner can be utilized to build a 4-channel combiner. For example, a two stages power combiner is shown in Fig 3.6. In this combiner, the characteristic impedance on each transmission line sections listed in the figure are selected for matching the PA with optimum load Z_{opt} if all the channels are in phase. The first stage, from plane A to plane B, is consist of two parallel Chireix Combiners. A quarter wavelength transmission line is placed between the first junction and each PA output. From plane B to

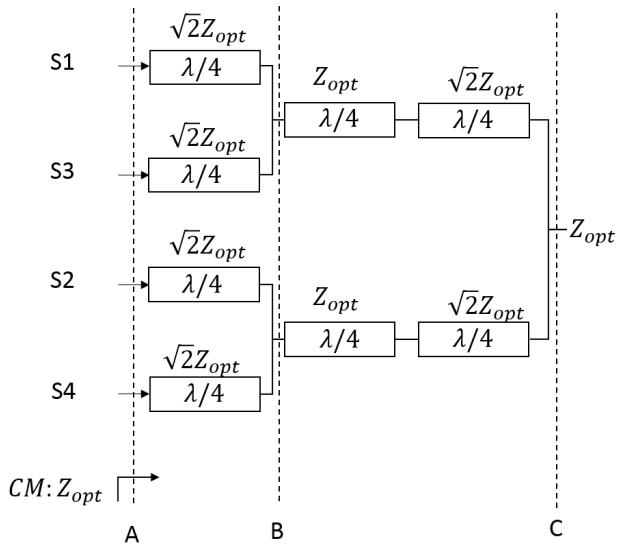

Figure 3.6: Two stages 4-channel combiner used for CANE

plane C, the second stage is a 2-way Chireix Combiner with two input branches extended by an additional quarter wavelength line. In the filter rejection band, these transmission lines perform as impedance inverters. The equivalent short circuit at plane B created by out of phase combining of S1 and S3 or S2 and S4, will be transformed to open circuits at plane A. Also, if the top two branches have 180 degree phase difference with the bottom two, then an equivalent short circuit is formed at plane C. However, the two sections of quarter wavelength line between B and C keep the short circuit profile at plane B, which is later converted to open circuit at plane A.

Fig 3.7 shows an example of 4-channel CANE with such combiner. At the first pair of nulls, the relative phase of "ch1" "ch2" "ch3" and "ch4" are 0^o,90^o,180^o and 270^o respectively. So either the top two branches or the bottom two branches are combined out of phase. However, at the second pair of nulls, the relative phases of the four channels become 0^o,180^o,0^o and 180^o. The top two signals "ch1" and "ch3" are now in phase, but they are opposite to the bottom two signals. So the four signals are canceled by each other at plane C.

Similar to the analysis shown in 2-channel case, we can investigate the equivalent load impedance through S-parameters. Let the port 1 be the combining port, the rest 4 ports are

input port, then the 4-channel combiner has a S-parameter matrix:

$$[S] = \begin{bmatrix} 0 & j/2 & j/2 & j/2 & j/2 \\ j/2 & 3/4 & -1/4 & -1/4 & -1/4 \\ j/2 & -1/4 & 3/4 & -1/4 & -1/4 \\ j/2 & -1/4 & -1/4 & 3/4 & -1/4 \\ j/2 & -1/4 & -1/4 & -1/4 & 3/4 \end{bmatrix} \tag{3.20}$$

For the in band signal, the excitation voltages are:

$$V^+] = [0, V_0, V_0, V_0, V_0]^T \tag{3.21}$$

Then the reflected waves are:

$$[V^-]] = [2jV_0, 0, 0, 0, 0]^T \tag{3.22}$$

So all the input ports are matched. At the first nulls, according the phase relations between these channels, the input waves are given by:

$$[V^+] = [0, V_0, -V_0, jV_0, -jV_0]^T \tag{3.23}$$

Then the out going waves are

$$[V^-] = [0, V_0, -V_0, jV_0, -jV_0]^T \tag{3.24}$$

The associated reflection coefficient of the four input ports are:

$$\Gamma_2 = \Gamma_3 = \Gamma_4 = \Gamma_5 = 1 \tag{3.25}$$

This means each of the PA is terminated by equivalent open circuit. At the second pair of nulls, we can apply same analysis and draw the same conclusion.

The two stages 4-channel combiner shown above can satisfy the load impedance modulation requirement in CANE. However, the structure consists of three sections of quarter wavelength line in each path, which may lead to higher insertion loss. Alternatively we can design a one stage 4-channel combiner, as shown in Fig 3.8. Now only one quarter wavelength line operates as impedance transformer between the PA output and combining point. However, to match PA with optimum load, the characteristic impedance of the transmission line should be higher. In some popular circuit type, such as microstrip line, the higher impedance often leads to narrower line width, which may also increase the loss.

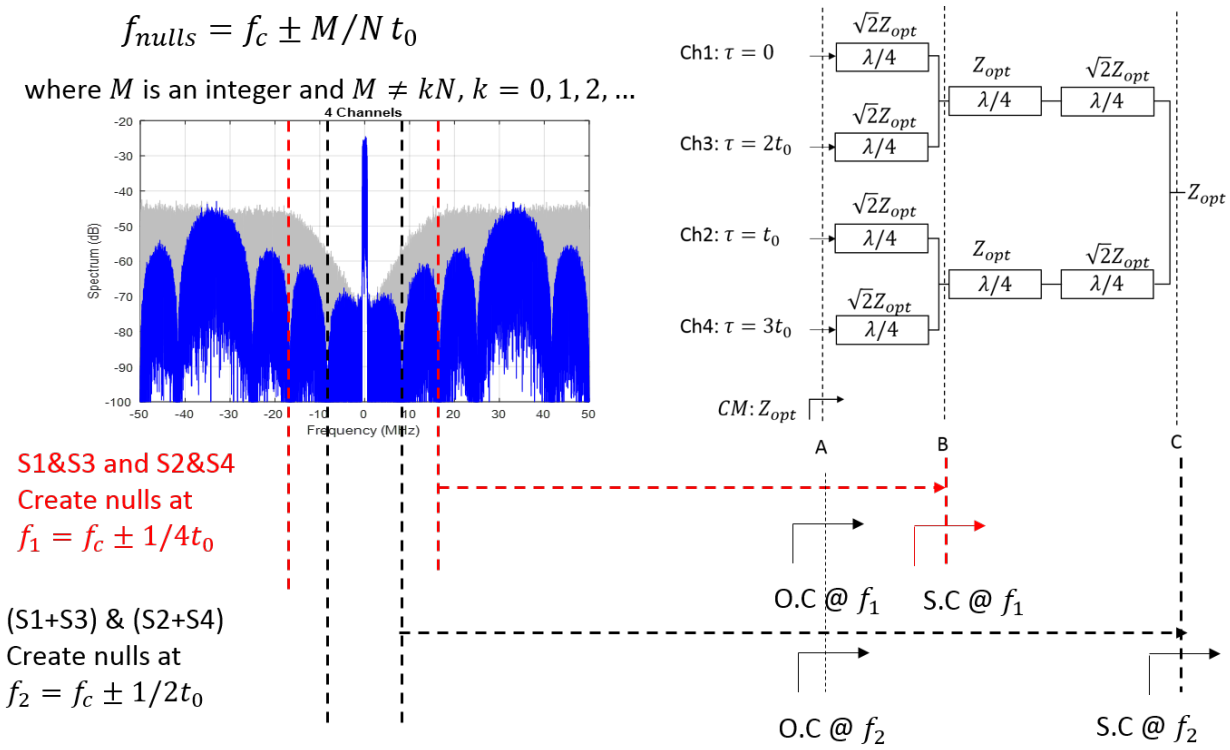

Figure 3.7: Operation Principle of 4-channel CANE

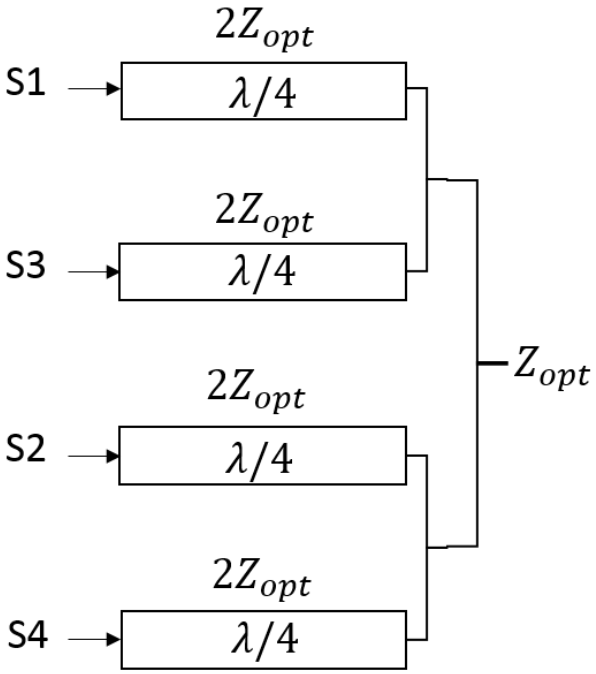

Figure 3.8: One stage 4-channel combiner used for CANE

3.4.4 Further discussion of load modulation

In previous discussion, we analyze the load impedance of the PAs when they are combined completely in phase or out of phase. As mentioned before, these two statuses mainly determine the overall system efficiency. However, the investigation on the load impedance when the quantization noise is partially suppressed might provide additional guidance for designing the power combiner.

For example, in a 2-channel combiner, let the input signal be

$$[V^+] = [0, V_0, V_0 e^{j\Omega}] \tag{3.26}$$

where Ω is the normalized phase shift in the second channel,

$$\Omega = 2\pi t_0 (f - f_c) \tag{3.27}$$

The outgoing wave in terms of phase difference can be expressed as:

$$V_2^- = \frac{1}{2} V_0 (1 - e^{-j\Omega}) \tag{3.28}$$

$$V_3^- = \frac{1}{2} V_0 (-1 + e^{j\Omega}) \tag{3.29}$$

The reflection coefficient of each input port is then:

$$\Gamma_{2,3} = \frac{V_{2,3}^-}{-_{2,3}} = \pm \frac{1}{2} (1 - e^{j\Omega}) \tag{3.30}$$

We can plot the trajectory of the impedance seen by PA output. Fig 3.9 plots the equivalent input impedance of port 2 and port 3 in the 2-channel combiner on Smith Chart. The trajectory locates on the right half of the chart, which has larger absolute value of impedance. So with constant voltage sources, the current injected to the ports is reduced.

For 4-channel combiner, using the delay assignment as shown in Fig 3.7, the input voltage is:

$$[V^+] = [0, V_0, V_0 e^{j2\Omega}, V_0 e^{j\Omega}, V_0 e^{j3\Omega}] \tag{3.31}$$

and the out going wave is:

$$V_2^- = V_0 (1 - \frac{1}{4} \frac{sin(2\Omega)}{sin(\frac{\Omega}{2})} e^{j\frac{3}{2}\Omega}) \tag{3.32}$$

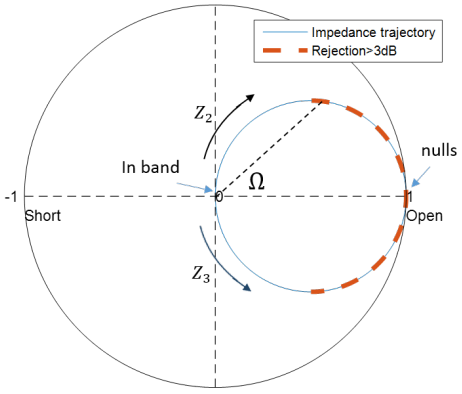

Figure 3.9: Impedance trajectory of 2-channel combining

$$V_3^- = V_0(e^{j2\Omega} - \frac{1}{4}\frac{sin(2\Omega)}{sin(\frac{\Omega}{2})}e^{j\frac{3}{2}\Omega}) \tag{3.33}$$

$$V_4^- = V_0(e^{j\Omega} - \frac{1}{4}\frac{sin(2\Omega)}{sin(\frac{\Omega}{2})}e^{j\frac{3}{2}\Omega}) \tag{3.34}$$

$$V_5^- = V_0(e^{3j\Omega} - \frac{1}{4}\frac{sin(2\Omega)}{sin(\frac{\Omega}{2})}e^{j\frac{3}{2}\Omega}) \tag{3.35}$$

So the reflection coefficient of each port is:

$$\Gamma_2 = 1 - \frac{1}{4}\frac{sin(2\Omega)}{sin(\frac{\Omega}{2})}e^{j\frac{3}{2}\Omega} \tag{3.36}$$

$$\Gamma_3 = 1 - \frac{1}{4}\frac{sin(2\Omega)}{sin(\frac{\Omega}{2})}e^{j\frac{-1}{2}\Omega} \tag{3.37}$$

$$\Gamma_4 = 1 - \frac{1}{4}\frac{sin(2\Omega)}{sin(\frac{\Omega}{2})}e^{j\frac{1}{2}\Omega} \tag{3.38}$$

$$\Gamma_5 = 1 - \frac{1}{4}\frac{sin(2\Omega)}{sin(\frac{\Omega}{2})}e^{j\frac{-3}{2}\Omega} \tag{3.39}$$

We can plot the reflection coefficients or associated impedance on smith chart, as shown in Fig 3.10.

Different from the the 2-channel case, the impedance trajectory in 4-channel combiner has two patterns. This is because phase changing rates of port 3 and port 4 are doubled as port 2 and port 5. But in either of the patterns, the impedance for the rejection band falls into the high impedance region. Another interesting observation is that part of the reflection

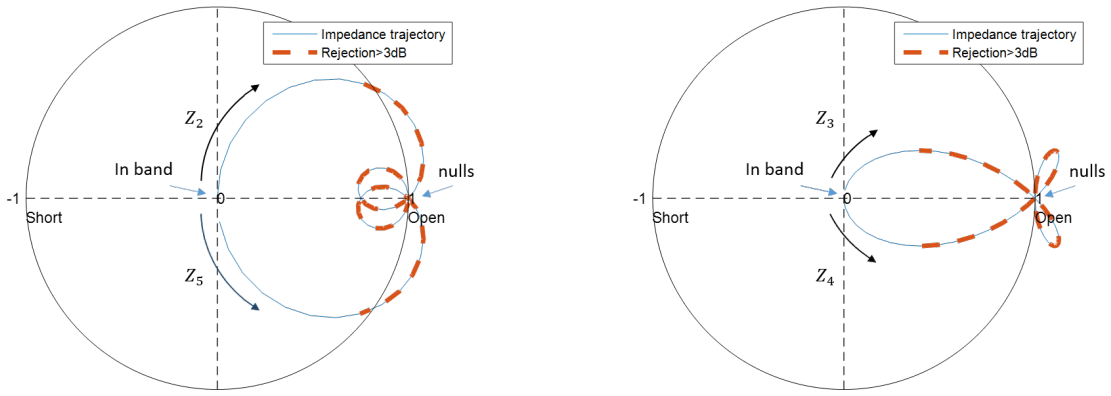

(a) (b)

Figure 3.10: Impedance trajectory of 4-channel combining. (a) Impedance of port 2 and port 5. (b) Impedance of port 3 and port 4

coefficient exceeds beyond unit circle in Smith Chart, which means that the the noise power reflected to the PA is stronger than its output. However, this amount of noise is equivalently recycled to power supply and the power efficiency is preserved.

3.5 Implementation of CANE

Previous sections discuss the noise suppression in CANE system and the principle of preserving the system power efficiency. We can see that CANE is a composite architecture and requires design from system level to circuit implementation. This section will present an implementation of CANE system.

3.5.1 System Design

To verify the concept, we fabricated two EDSM transmitters module for two channels and fours channels CANE. The diagram of the overall system setup is shown in Fig 3.11. The bitstream modulated signal is transferred from PC to AWG through GPIB port. The signal generation module is controlled by PC through USB-SPI controller. The four channels RF signal are pre-amplified by four identical driver amplifier TQP9111 and fed into the PA

modules. The output power and spectrum are measured simultaneously.

As a benefit of CANE technique, all the signal processing can be accomplished in baseband DSP. The envelope delta sigma modulation of the complex baseband signal is accomplished in PC. The I and Q path of this bitstream modulated signal is output from Tektronix arbitrary waveform generator AWG520 and sampled to a FPGA based signal processing module. The FPGA chip is used as the main controller of the system and can support four parallel outputs with real time delaying operation. The analogue baseband signal is sampled by an ADC into the FPGA internal memory with sampling rate of 100 MSps. The delaying is conducted by reading the data in an offset memory address. Due to the sampling rate, the delaying resolution is 10 nS. The complex baseband signals are then output from four pairs of DACs to a block of mixers and up-converted to the same carrier. Besides the delay in each channel, the RF signal amplitude, carrier frequency and phase offset are also tuned by FPGA.

In the experiment, we tested both two channels and four channels CANE with a QPSK signal and a LTE signal. The symbol rate of the QPSK signal is 1 MSps. The signal pulse is shaped by a square root raised cosine filter with roll-off factor of 0.2, so its bandwidth is 1.2 MHz and the PAPR is 5.3 dB. The sampling rate is chosen as 100 MSps to match the sampling speed of the ADC in the signal generation module. Both two levels and three levels EDSM are used to generate the bitstream modulated envelope. The spectrum and power efficiency of the output signal with or without delaying are measured and compared. The delay length is selected to be 200 nS, which places the first null 2.5 MHz offset from the center frequency. In addition, a 1.4 MHz LTE signal with 10 dB PAPR is also tested for evaluating the performance of noise suppression and efficiency preservation under high PAPR situation.

3.5.2 PA design

First of all, The Pulsed Load Modulation PA is the fundamental building block of the bitstream modulated transmitter because the power efficiency is essentially enhanced by its

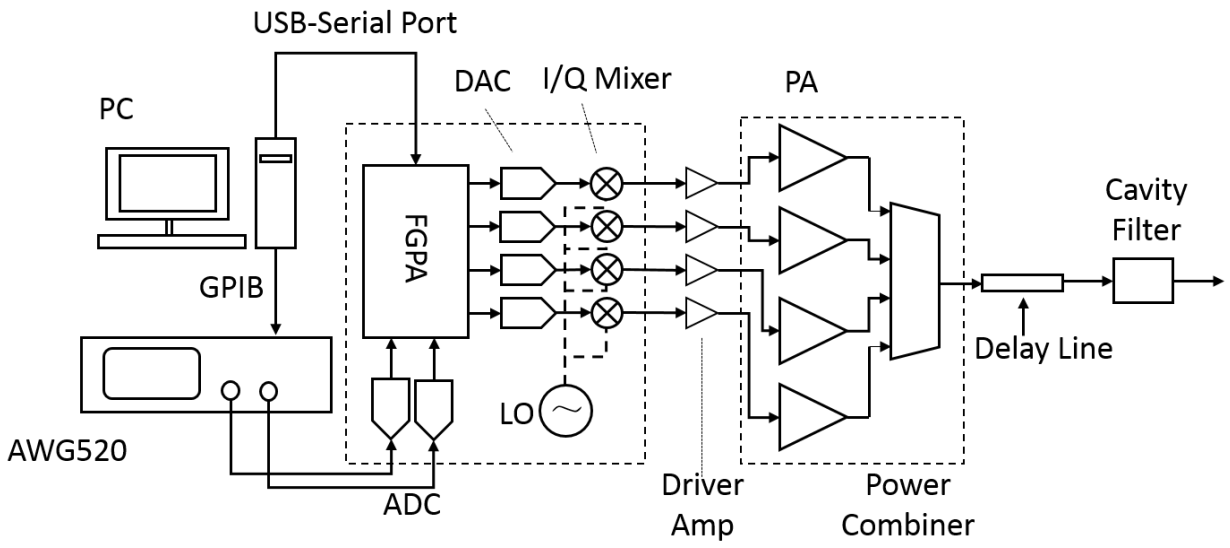

Figure 3.11: System Design of CANE

dynamic load impedance modulation. The PLM PA with a output filter forms a switched resonator structure which preserves the system efficiency while suppress the far out quantization noise. The topology of PLM PA is similar to a Doherty PA, but to create a RF switching voltage source, the design of PLM PA matching circuit require special consideration. First, whether the PA is turned on or off, the output impedance should be relatively small to emulate a voltage source. Second, when the PA output is terminated by high impedance, the transistor drain point should also see high impedance so the total drain current is reduced. The first condition can be satisfied by choosing appropriate device, such as III-V pHemt transistor. The second condition can be achieved by designing the output matching network. In this work, each PLM PA unit is consist of two Wolfspeed CGH40010 GaN transistors with the drain voltage supply of 28V. The schematic of one PLM unit used in this experiment is shown in Fig 3.12.

In the output matching network, a shunt transmission line with characteristic impedance of Z_1 and electric length of θ is used to resonant the parasitic capacitance C_{ds} of transistors. So the optimum impedance R_{opt} at the drain point becomes a real number. The quarter wavelength line with impedance of Z_2 transforms R_{opt} to 50Ω. So at the output port of this block, the optimum impedance is 25Ω. In fact, similar to the "inverse Doherty PA",

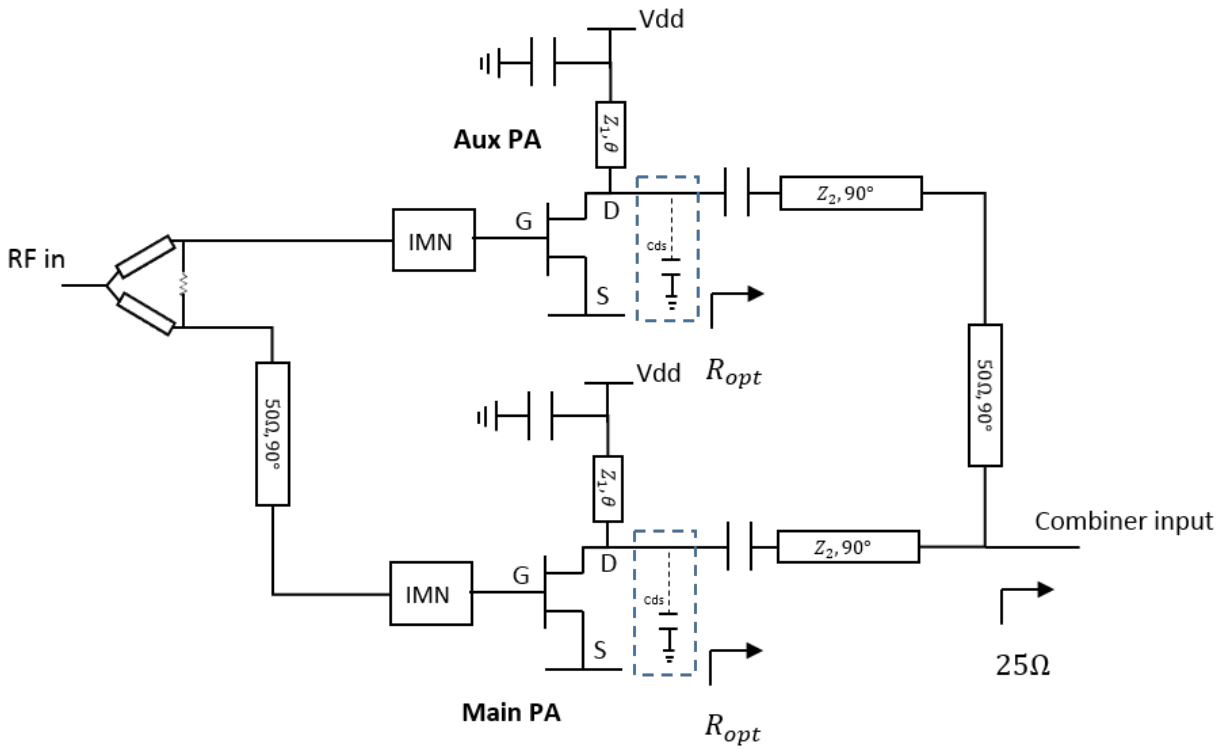

Figure 3.12: Schematic of PLM unit used in the experiment

the proposed schematic implements a "inverse PLM PA". Different from conventional PLM PA, the 50Ω line is inserted between the the combining point and the auxiliary PA output, rather than the main PA.

When the PAs are turned on, the auxiliary PA presents low output impedance. While the two sections of quarter wavelength line keep the low impedance at the junction. When the PAs are turned off, the high output impedance from the main PA is converted to low impedance by the quarter wavelength line in its matching network.

3.5.3 Combiner design

Based on the output impedance of the PA, we can design the power combiners. In the 2-channel combining case, a modified Chireix combiner is used in this work. Fig. 3.13 shows the diagram of the proposed 2-channel combiner. The output of the combiner is connected to a cavity filter through a 50Ω offset line. The electric length of the offset line is used to

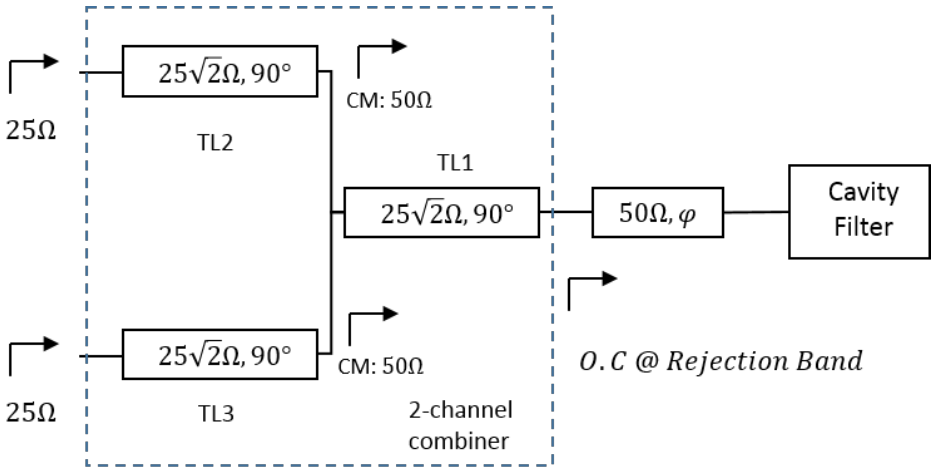

Figure 3.13: Schematic of 2-channel Combiner

ensure a high impedance load in the cavity filter rejection band. For the in band signal, TL1 converts 50Ω load to 25Ω at the junction. Due to the common mode excitation, each of the two branches sees 50Ω. Then TL2 and TL3 play another round of impedance transformation and each of the PLM unit is terminated by 25Ω.

Similarly, the 4-channel combiner is modified to match the designed PLM PA. The two stages 4-channel combiner is employed in this project because it is easier to be integrated with PA circuits. Fig 3.14 shows the proposed 4-channel combiner and Fig 3.15 shows the picture of the fabricated PA modules.

3.6 Experiment

3.6.1 PLM PA efficiency

In this experiment, single PLM unit can output a maximum power about 38.4 dBm with a maximum power efficiency of 67% with de-embedded the 0.5 dB insertion loss of the output cavity filter. With considering the loss from the filter, the peak power efficiency is above 60%. The measured power efficiency of two combined PA units is shown in Fig.3.16. The efficiency of the PLM mode is compared with biasing the PA as conventional class-B mode. Since the PLM PA is driven by a train of constant envelope pulses, the different output

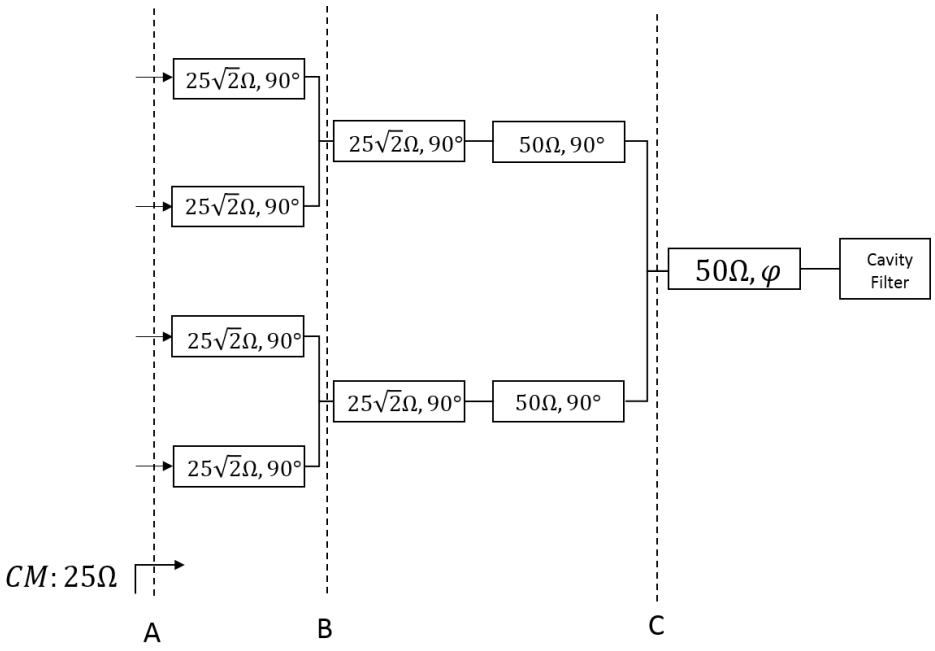

Figure 3.14: Schematic of 4-channel Combiner

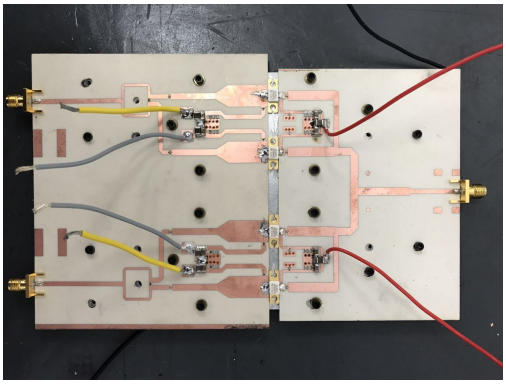

(a)

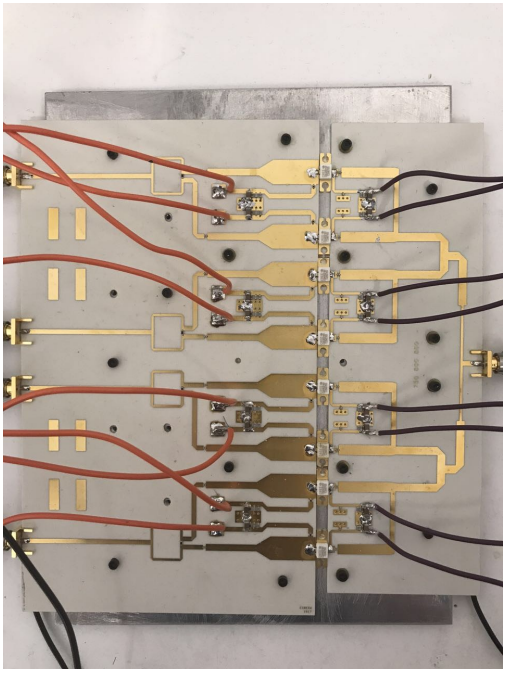

(b)

Figure 3.15: Picture of PLM PA used in CANE. (a)2-channel combining. (b)4-channel combining

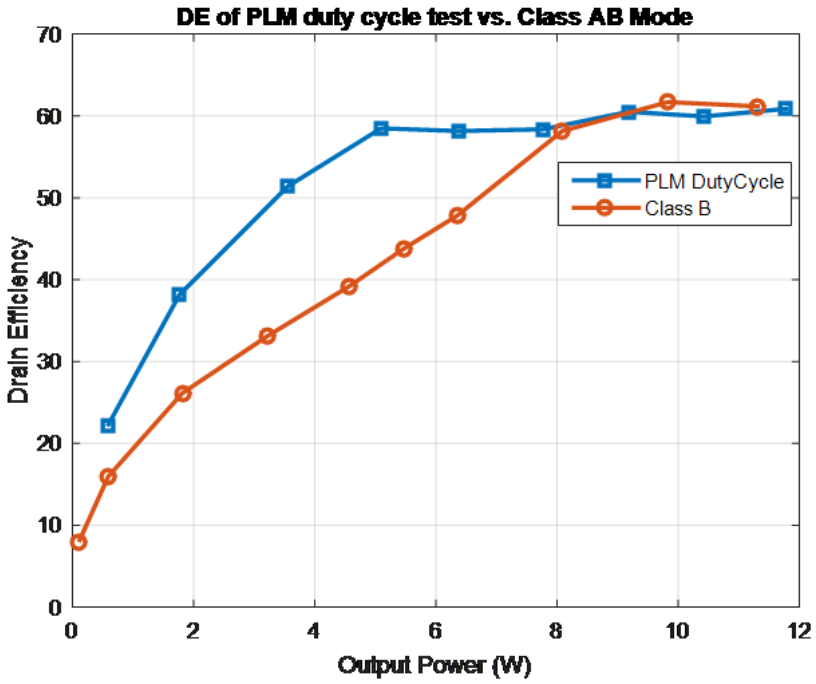

Figure 3.16: System Design of CANE

power is achieved by varying the pulse duty cycles from 100% to 0%. From the curves, it can be seen that the PLM mode can improve the efficiency at output power back-off up to 6dB.

3.6.2 2-channel noise suppression

Fig 3.17 shows the measured spectrum with two channels combining module for QPSK signal, and Fig 3.18 shows the measurement result for LTE signal. The in band signal linearity is preserved by EDSM noise shaping and the measured ACLR is about 32 to 33 dBc. Noise performance of different cases with the 2-level or 3-level EDSM, with and without applying CANE are compared. First of all, the 3- level EDSM produces less quantization noise than 2-level case. For example, in the QPSK test the noise at 20 MHz offset in 2-level EDSM is about 22 dBc below the in band signal, while the 3-level EDSM has the noise level about -30 dBc at the same frequency. Second, the noise suppression from CANE is obviously shown in the spectrum plot. As the delay time is set to be 200 nS, we can see that the first null

locates at 2.5 MHz offset from the center. Futhermore, the periodical stopbands can also be observed in the plot.

For this two PAs combining module, the signal to quantization noise ratio and in band signal occupation with the analogue filter passband are calculated and listed in Table 3.1. For QPSK signal with 2-level EDSM, CANE improves the SQNRF from 7.13 dB to 10.53 dB and in band signal occupation from 83.81% to 91.87%. For the 3-level EDSM test, the SQNRF with and without CANE is 13.45 dB and 16.52 dB respectively. The SQNRF improvement is smaller in 3-level envelope modulation, because the quantization noise generated by the multi-level EDSM is intrinsically smaller than the 2-level case.

Similar improvement on SQNRF can be seen in the LTE test. The SQNRF improvement in 2-level and 3-level EDSM cases are 2.12 dB and 2.06 dB respectively. Since the LTE signal has high PAPR, it requires larger oversampling ratio to reduce the quantization noise. So the LTE signal has higher noise level than QPSK. This phenomenon is more obvious in 3-level EDSMs. Comparing the noise at 20 MHz offset, the noise level in QPSK is -30 dBc, but in LTE signal, the noise level is -25 dBc. Therefore, with limited sampling rate, the high PAPR signal requires stronger noise suppression method, such as multi-channels CANE filter.

3.6.3 4-channel noise suppression

The four PAs combining module is used to test with LTE signal for evaluating the multi-channel noise suppression. Fig 3.19 shows the measured spectrum. The 4-channel combining CANE is compared with the 2-channel combining case and the original EDSM. The two channels combining in this test is created by setting two channels with zero delay and the other two with 100 nS delay. The delay unit in the four channels combining test is 30 nS, so the delay lengths assigned to each channel are 0 nS, 30 nS, 60 nS and 90 nS.

In the spectrum of 2-channel combining CANE, it can be seen that the first pair of nulls appears at 5 MHz offset from the center frequency. The higher order stopband then incurs every 10 MHz offset from the first null. However, the second and third order passbands of the FIR filter fall into the analogue filter, in which quantization noise is not fully suppressed.

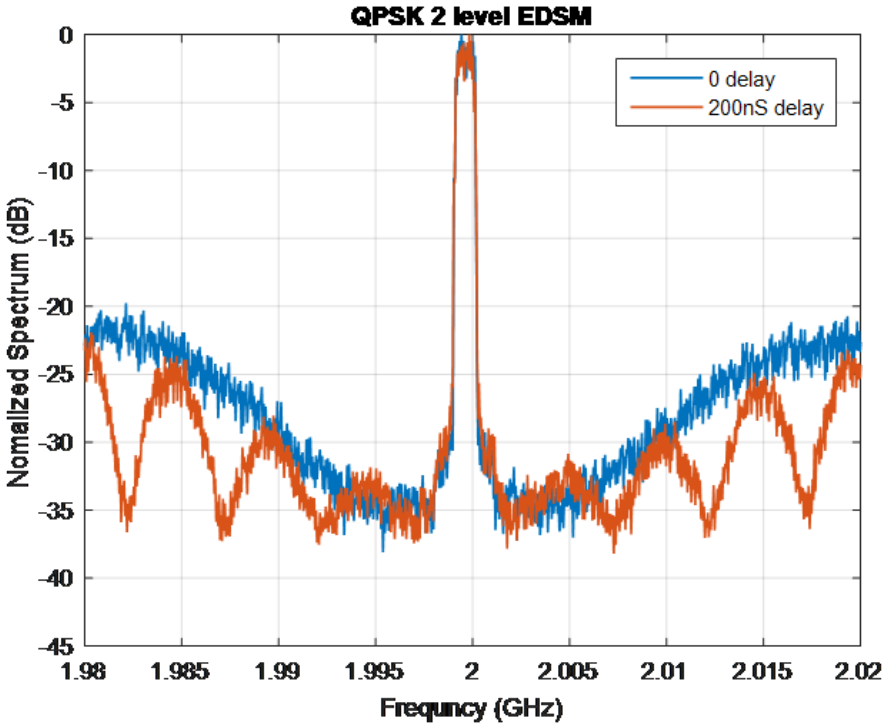

(a)

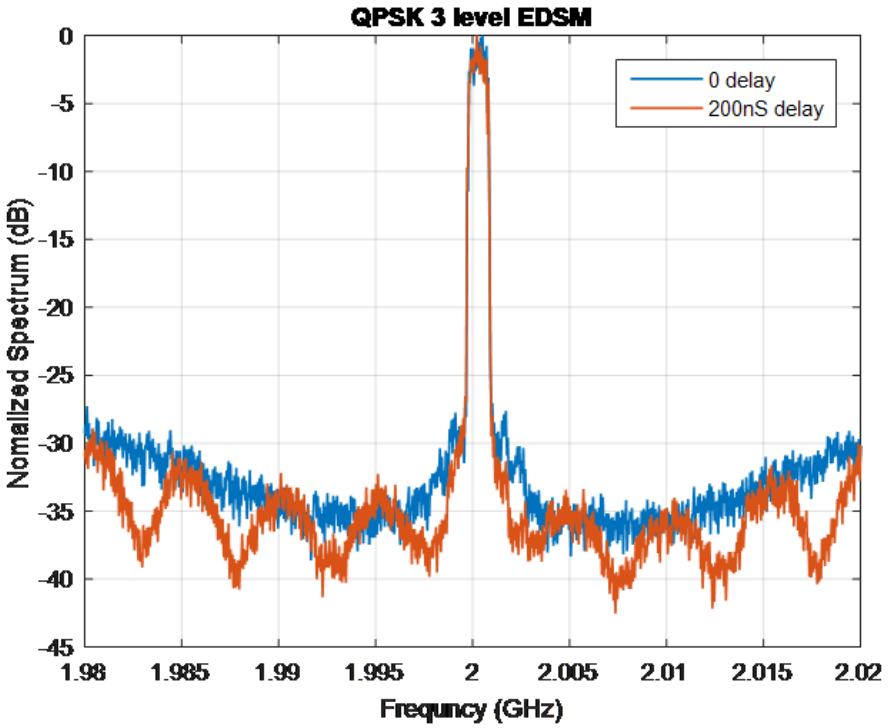

(b)

Figure 3.17: Measured spectrum of two combined PLM PA units with QPSK signal. (a) 2-level EDSM (b) 3-level EDSM

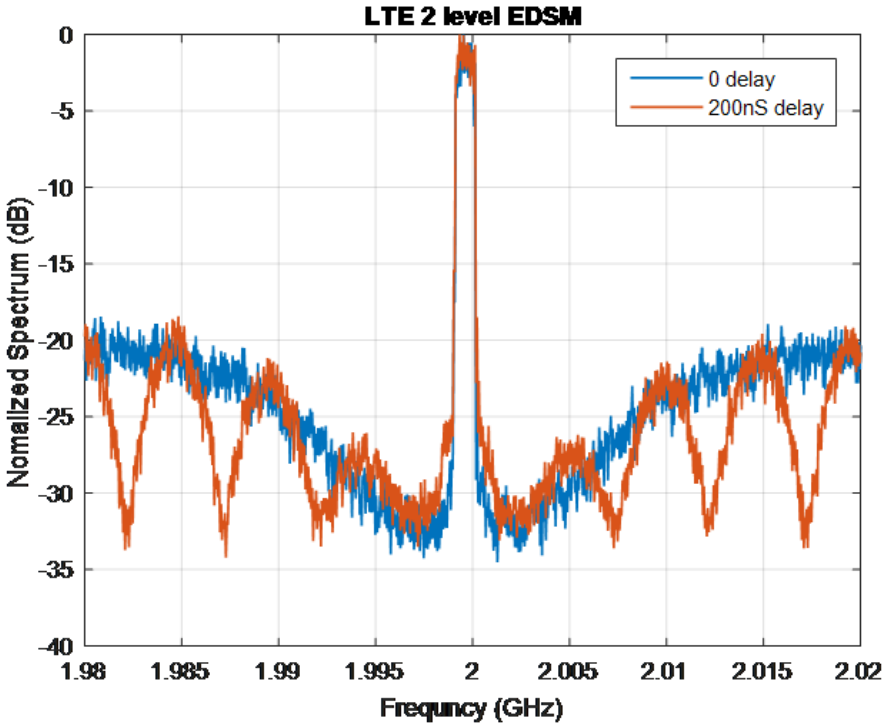

(a)

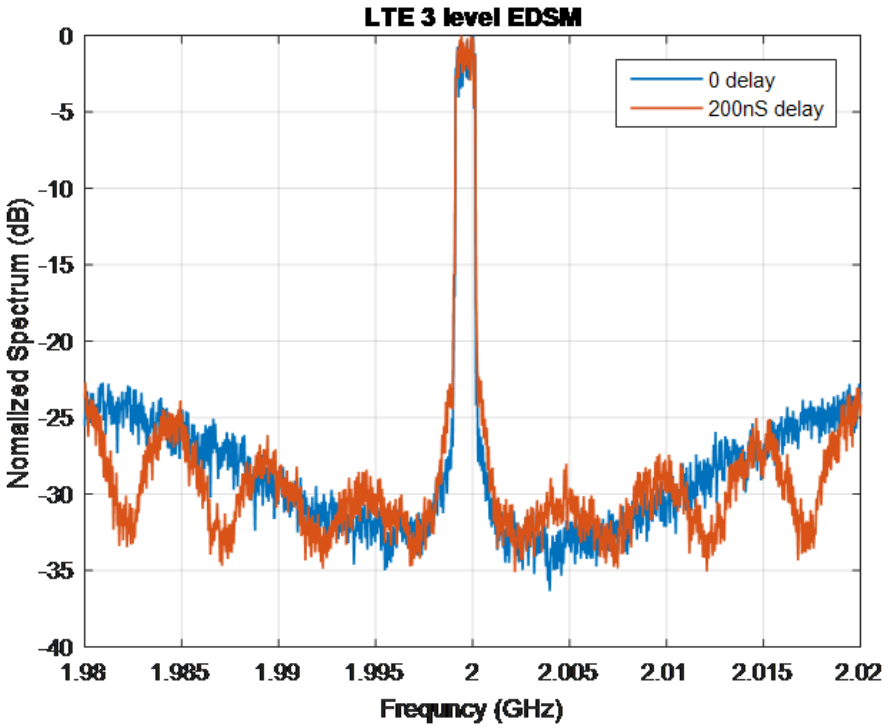

(b)

Figure 3.18: Measured spectrum of two combined PLM PA units with LTE signal. (a) 2-level EDSM (b) 3-level EDSM

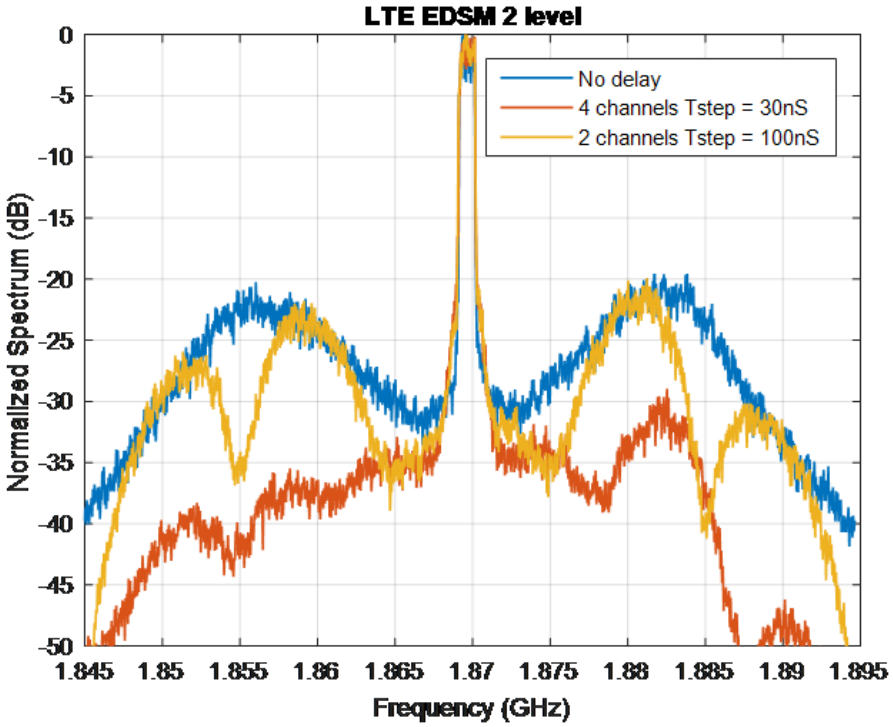

(a)

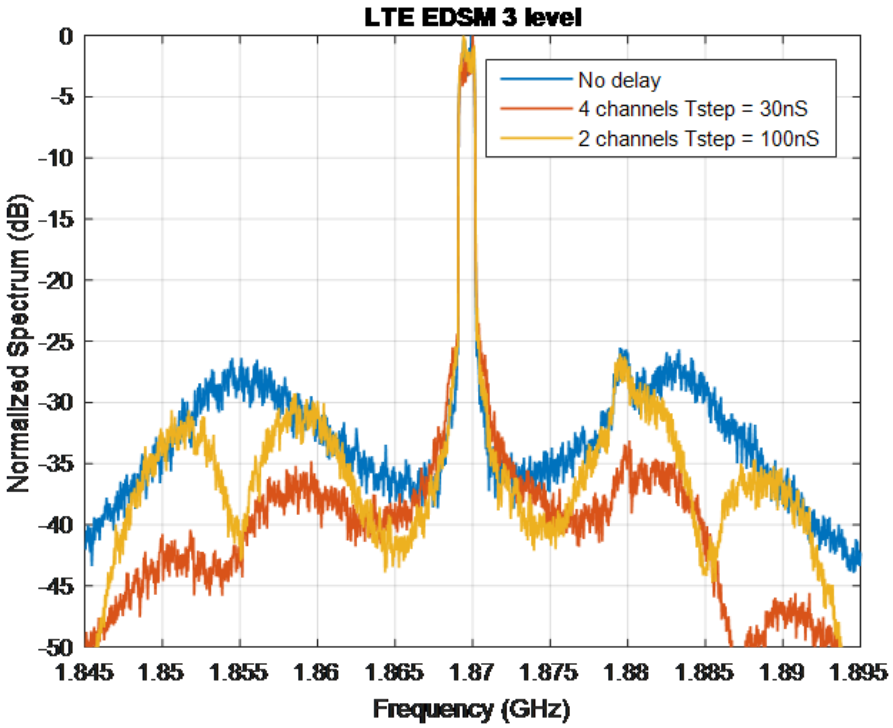

(b)

Figure 3.19: Measured spectrum of four combined PLM PA units with LTE signal.(a) 2-level EDSM (b) 3-level EDSM

However, the 4-channel combining provides a much better noise suppression because of its wider stopband. In the meantime, the higher order passband in 4-channel CANE is placed out of the analogue filter passband. So the quantization noise remained is better rejected.

Table 3.2 shows the calculated SQNRF and in band signal occupation of each case. For the 2-level EDSM, the 2-channel CANE improves the SQNRF by 3.17 dB, while the 4-channel combining improves SQNRF by 10.93 dB. For the 3 level EDSM, the 2-channel CANE increases SQNRF by 2.7 dB, while the 4-channel case improves it by 5.33 dB. Again, we can see the multi-channel CANE achieves better noise suppression.

3.6.4 Power Efficiency with CANE

3.6.4.1 Efficiency of 2-channel CANE

The measured output power and efficiency of the two PAs combining module are listed in Table 3.2. For the QPSK signal, the 2 level EDSM case has output power of 37.94 dBm and overall efficiency of 53.8% without CANE. With 2-channel CANE, the output power and efficiency become 37.6 dBm and 52.1%, which remain at the same level as those without noise cancellation. However, as quantization noise is suppressed, the effective efficiency of the desired signal can be even higher. Define the estimated effective efficiency of in band signal as the product of overall efficiency and the percentage of desired signal out of the whole spectrum. Then the calculated effective efficiency before and after CANE are 45.1% and 47.8% respectively. This implies that the quantization noise is indeed rejected in a power saving mode.

In the 3 level EDSM test with QPSK, the output power increased to 39.53 dBm without CANE and 39.38 dBm with CANE. The power efficiency also increases to about 60%. This multi-level EDSM itself indeed improves both the output power and efficiency, because it produces less quantization noise in the bitstream modulation and more power concentrates in the desired signal. Also, the noise power needs to be rejected is smaller than the 2 level case.

QPSK signal with PAPR of 5.3 dB					
EDSM level	Noise Filter	Pout (dBm)	Efficiency	SQNRF (dB)	In band signal
2 level	BPF only	37.94	53.8%	7.13	83.81%
2 level	BPF+2-ch CANE	37.6	52.1%	10.53	91.87%
3 level	BPF only	39.53	59.9%	13.45	95.68%
3 level	BPF+2-ch CANE	39.38	60.4%	16.52	97.82%
LTE signal with PAPR of 10 dB					
EDSM level	Noise Filter	Pout (dBm)	Efficiency	SQNRF (dB)	In band signal
2 level	BPF only	35.95	53.24%	4.37	73.24%
2 level	BPF+2-ch CANE	35.77	49.75%	6.49	81.66%
3 level	BPF only	36.69	51.92%	8.52	87.66%
3 level	BPF+2-ch CANE	35.64	49.95%	10.58	91.96%

Table 3.2: Measured output power and efficiency of two PAs combined module

LTE signal with PAPR of 10 dB					
EDSM level	Noise Filter	Pout (dBm)	Efficiency	SQNRF (dB)	In band signal
2 level	BPF only	40.1	49.38%	7.16	83.86%
2 level	BPF+2-ch CANE	40.82	50.33%	10.33	91.52%
2 level	BPF+4-ch CANE	40.98	48.88%	18.09	98.48%
3 level	BPF only	41.25	46.78%	13.32	95.56%
3 level	BPF+2-ch CANE	42.18	47.19%	16.02	97.56%
3 level	BPF+4-ch CANE	41.67	46.42%	18.65	98.66%

Table 3.3: Measured output power and efficiency of four PAs combined module

3.6.4.2 Efficiency of 4-channel CANE

The power and efficiency measurement of the four PAs combining module with LTE signal is listed in Tabel 3.3. For the 2 level EDSM signal, the output power and efficiency before active noise filtering are 40.1 dBm and 49.38%. The output power with active noise cancellation slightly increases by about 0.71 dB to 0.88 dB with two channels and four channels CANE respectively, while the power efficiency remains at the same level. The effective efficiency of the in-band signal is 41.41% in the non-delaying case, 46.06% in two channels combining and 48.14% in four channels combining. Therefore, considering the noise suppression, the four channels combining achieves the best effective efficiency among the three settings. This means that the four channels power combiner in this module indeed provides appropriate load modulation scheme and recycles the quantization noise power.

Similar to the two PAs combining test, the 3 level EDSM LTE signal has slightly lower efficiency due to its high PAPR. But the power efficiency is still preserved with noise cancellation.

3.7 Discussion

Previous section presents the measurement results of CANE and proves that the active filter can improve the signal integrity in a bitstream modulated transmitter with preserving system power efficiency. The two PAs combining module operates at 1.995 GHz and the four PAs module works at 1.87 GHz, but the center frequency of the equivalent BPF does not need to adjusted because essentially it is co-located with the desired signal. In fact, as long as all the RF channels are identical, the equivalent filter characteristics are not sensitive to the delay variations. In addition, thanks to the decoupling of the filter response and LO frequency, CANE has a potential to be used as tunable filter in the multi-carrier system.

From the noise suppression measurement of two channels and four channels combining, filter capability of CANE is observed. In the spectrum simulation, the SQNR increases by about 3 dB with two channels CANE and more than 6 dB with four channels CANE.

Considering the noise performance with analogue filter, the SQNRF increases by more than 12 dB with four channels CANE. The improvement of SQNRF is proved by the experimental result.

Besides noise suppression, the load modulation scheme preserves the system power efficiency. Because the power combiners provide high impedance to the PAs at the out of phase combining point, CANE shows a current rejection filter to the RF voltage source. The measured power efficiency with and without CANE are approximately same. So the quantization noise is reflected to PA and its power is not wasted. Furthermore, the measured output power with CANE stays at approximately same or becomes even larger in some cases. For example, in the four channels combining test, the output power increases by 0.88 dB after turning on noise cancellation. One possible reason is that more drain current is allocated to the in band signal as the current associated with the noise is reduced. In the meantime, because the desired signal has larger power density, its power efficiency per hertz is higher than the noise. Therefore, the efficiency preservation phenomenon in CANE can be explained in the following two aspects: first, the noise power and associated drain current are reduced simultaneously; second, these amount of rejected current is re-allocated to the desired signal whose power efficiency is better.

In the comparison of different levels of EDSM with LTE signal, the 3-level EDSM has a slightly lower efficiency than 2-level EDSM. In the 3 level modulation, the envelope has three levels, zero-level, middle-level, and full-level. The zero-level and full-level refer to pinch-off and saturation of the transistors respectively. Both of these two status has high efficiency. But the efficiency of the middle-level is smaller. Because of the 10 dB PAPR of the LTE signal, most of the envelope amplitude is less than half of the peak value. So the middle level in the digitized envelope sequences exists more frequently than the maximum level, which results in efficiency degradation. On the contrary, the digitized envelope mostly distributed in either zero or full level in the 3 level EDSM with QPSK due to a lower PAPR. So the PAs operate closer to the ideal switching-mode. But with considering the noise reduction by multi-level EDSM, the 3-level EDSM with QPSK may achieves higher effective efficiency.

3.8 Other Application

3.8.1 IM3 suppression

CANE technique was initially proposed to suppress the quantization noise in bitstream modulated transmitter. However, CANE essentially brings a baseband FIR filter to radio frequency, which can be applied to any transmitter. So in ordinary transmitter, CANE can be utilized to suppress some nonlinear distortions, such as third order intermodulations (IM3)

The principle of suppressing IM3 in CANE is to place the IM3 tones at the nulls of the active filter. For a given two tones signal, the CANE system can adjust its delay lines and shift the rejection band to IM3 frequencies. For simplicity, here we assumes the nonlinear distortions of a power amplifier can be described by Taylor expansion:

$$v_{out} = a_1 v_{in} + a_3 v_{in}^2 + a_5 v_{in}^5 + ... \tag{3.40}$$

where v_{in} is the input signal and v_out is the PA output. a_1 describes the linear gain of the fundamental tones. Here we only consider the odd order of nonlinear terms, because the nonlinear distortions from even order terms are further away from the fundamental tones and they are often rejected in differential structures. In addition, the third order intermodulation terms are generally determined by third order non-linear polynomial as a_3 is more significant than the other coefficients.

Consider the input signal as two tones sinusoid wave,

$$v_in = cos(\omega_c t + \omega_0 t) + cos(\omega_c t - \omega_0 t) \tag{3.41}$$

Where ω_c is the carrier frequency. The upper and lower side tones are placed at frequency $\omega_c + \omega_0$ and $\omega_c - \omega_0$ respectively. Then the output fundamental tones are:

$$v_1 = (a_1 + \frac{9}{4} a_3)[cos(\omega_c t + \omega_0 t) + cos(\omega_c t - \omega_0 t)] \tag{3.42}$$

And the IM3 tones can be expressed as:

$$v_{IM3} = \frac{3}{4} a_3^2 [cos(\omega_c t + 3\omega_0 t) + cos(\omega_c t - 3\omega_0 t)] \tag{3.43}$$

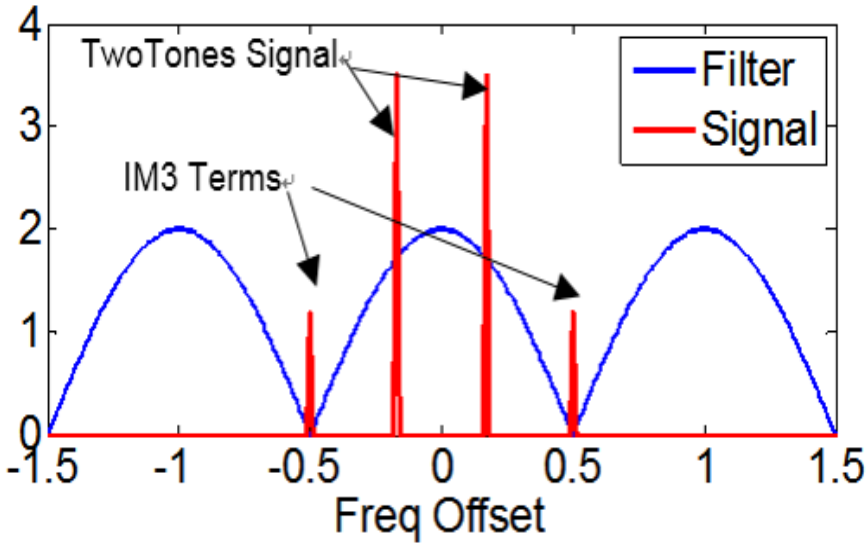

Figure 3.20: Example of the 2-channel CANE filter characteristic suppressing the IM spectrum components.

The IM3 tones then locates at frequencies:

$$\omega_{IM3} = \omega \pm 3\omega_0 \tag{3.44}$$

For instance, in 2-channel CANE, let the baseband delay length be

$$\tau = \frac{\pi}{3\omega_0} \tag{3.45}$$

Then the IM3 in the delayed channel is:

$$\begin{aligned} v_{IM3,delayed} &= \frac{3}{4}a_3^2[cos(\omega_c t + 3\omega_0 t - 3\omega_0\tau) + cos(\omega_c t - 3\omega_0 t + 3\omega_0\tau)] \\ &= -\frac{3}{4}a_3^2[cos(\omega_c t + 3\omega_0 t) + cos(\omega_c t - 3\omega_0 t)] \end{aligned} \tag{3.46}$$

which is opposite to the IM3 in the non-delayed channel. So by combining the two channels, IM3 can be canceled, as shown in Fig.3.20 Generally, if the input signals are two narrow band signals whose bandwidth is much smaller than the carrier frequency, the signal can be approximately modeled as two tones complex baseband signal

$$x(t) = e^{j\omega_1 t} + e^{j\omega_2 t} \tag{3.47}$$

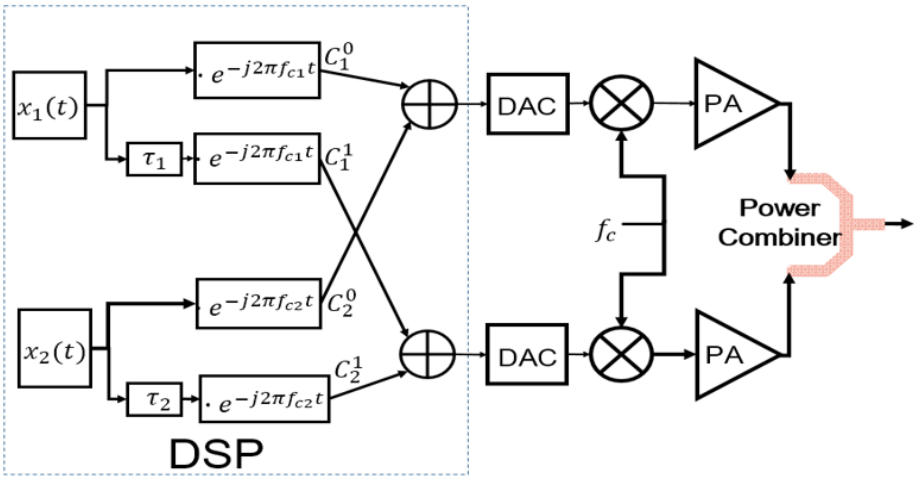

Figure 3.21: Diagram of the 2-channel multi-carrier CANE for multi-carrier IM3 suppression.

Then the IM3 tones are locate at $\omega_c + 2\omega_1 - \omega_2$ and $\omega_c + 2\omega_1 - \omega_2$. For the CANE filter, let the equivalent baseband FIR filter response be denoted by $H_B(\tau;\omega)$, we just need to solve to the delay timetau which satisfies:

$$H_B(\tau; 2\omega_1 - \omega_2) = 0 \tag{3.48}$$

And

$$H_B(\tau; 2\omega_2 - \omega_1) = 0 \tag{3.49}$$

The IM3 tones will be trapped in the filter rejection band.

Note that in this active filtering structure, the equivalent filter response is independent to the carrier frequency. The filter behavior is totally controlled by the baseband delay lines. Therefore, this allows us to implement the IM3 elimination for multi-carries systems with the same set of RF amplifier hardware. For each carriers, one can design the specific equivalent filter individually by varying its own baseband delay lines. Fig.3.21 shows a two carriers 2 channels IM3 suppression transmitter structure. Fig.3.22. shows the filtering characteristics of the two carriers IM3 suppression. One filter is synthesized with CANE for each carrier and each filter can work independently for its own purpose without interfering with each other. A total of M channels CANE can thus support a maximum of M carriers with a CANE filter for each of the carriers.

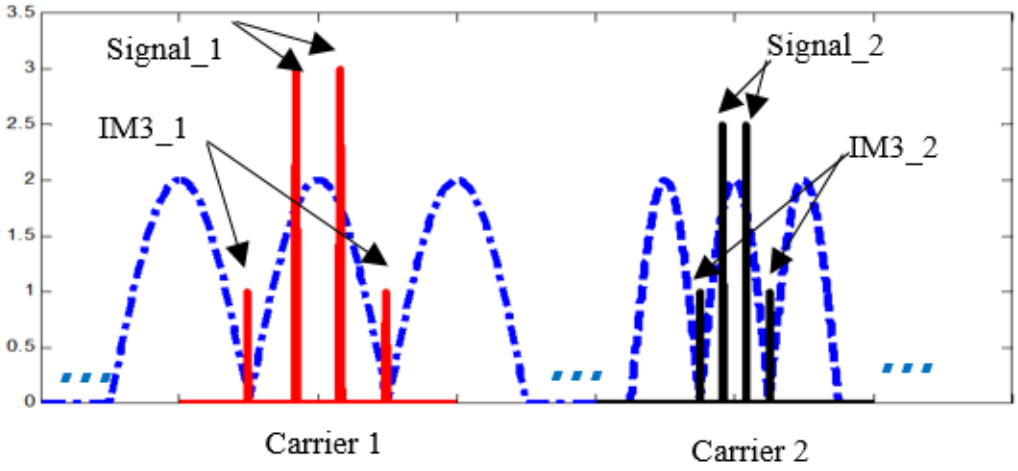

Figure 3.22: Example of the 2-channel CANE filter characteristic suppressing the IM spectrum components.

The IM3 suppression with CANE is validated with a two PA combined module. Fig 3.23 shows the diagram and picture of the circuits.The PA consists of two units of 7Watt amplifier with each of them being a Doherty amplifier. The center frequency of the operation is at 1.995GHz. The two channels IM3 suppression is tested with this transmitter and the results are used to demonstrate effect of this technique for both a single carrier input and a dual carriers input.

The baseband input is signal of 2 tones separated by 500KHz. The IM3 tones are thus located at 750KHz offset from the center. Fig. 3.24 shows the measured results. Without suppression technique, the IM3 level is about -15.4dB below the signal tones. However, after applying the proposed technique, the IM3 level is reduced to -32.64dB below the signal tones. Before suppression, the drain efficiency of PA is 57.42%, while after IM3 cancellation, the drain efficiency is 52.282%. The in-band signal power remains at approximately same level but the side tones are reduced.

The dual carriers IM3 suppression experiment uses the architecture shown in Fig. 3.21 The baseband input for both carriers are two tones spaced by 500 KHz. The two carriers are separated by 4.99 MHz. The first carrier is placed at 1.995GHz and the other is at

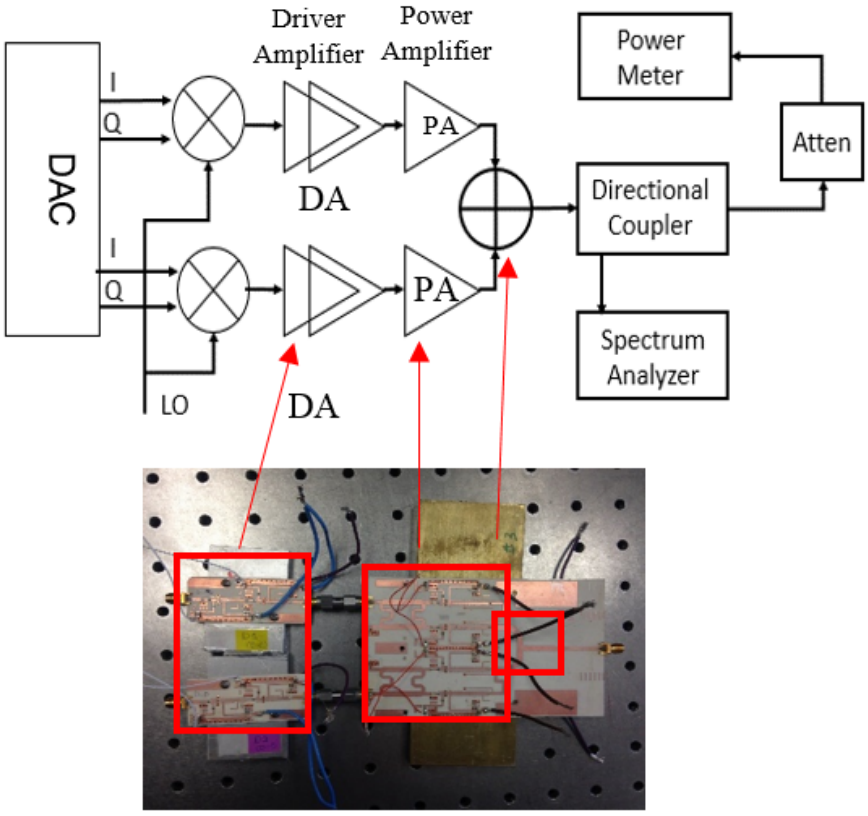

Figure 3.23: Diagram and picture of fabricated Doherty PA with two Channels CANE

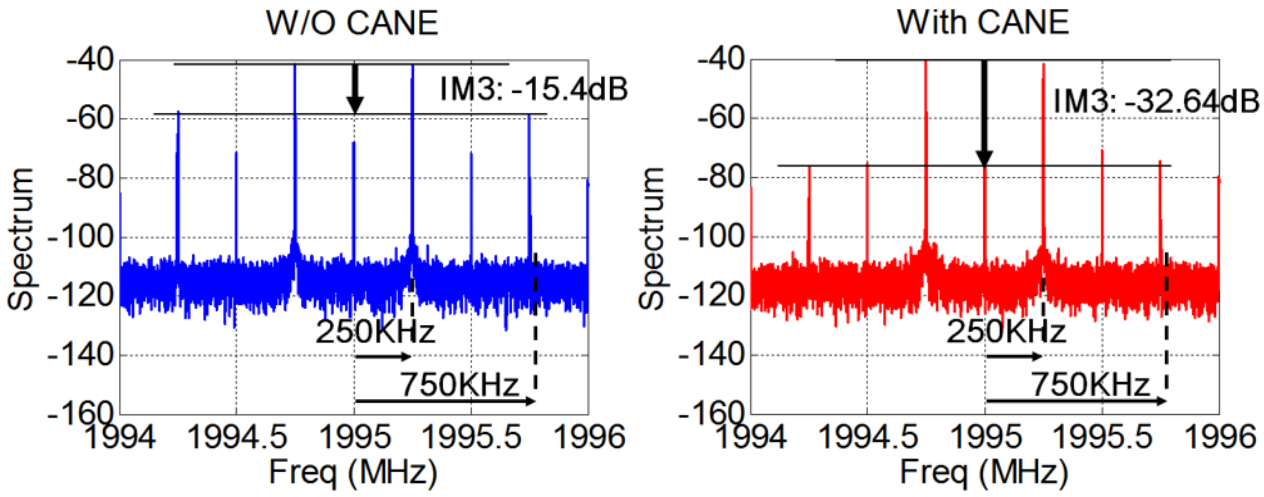

(a) (b)

Figure 3.24: Measured spectrum of a single carrier two-tone signal (a) before IM3 suppression with CANE (b) after IM3 suppression with CANE. 17dB overall IM3 suppression is observed.

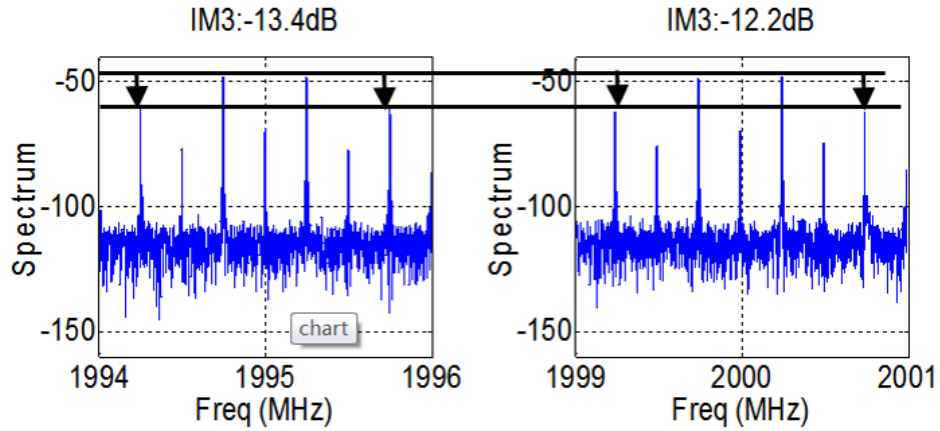

(a)

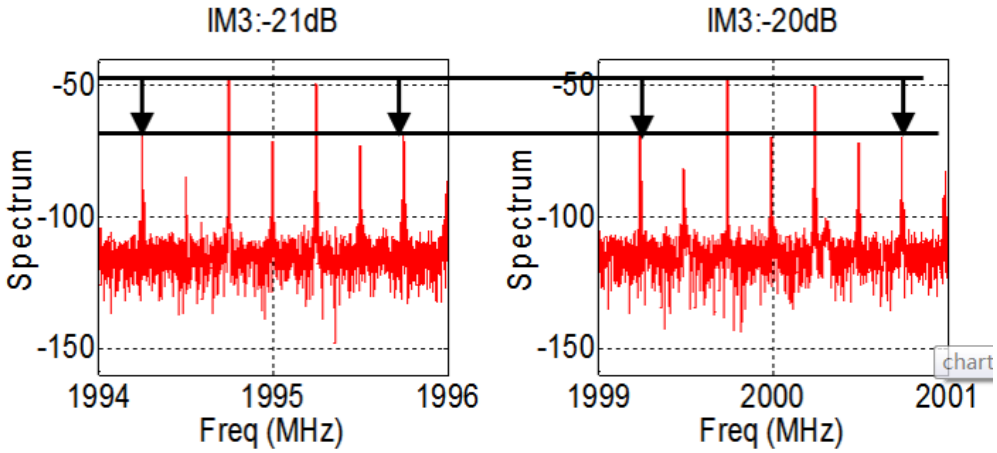

(b)

Figure 3.25: Spectrum Measurement of the two-carrier with two-tone signal (a) before IM3 suppression with CANE (b) after IM3 suppression with CANE.

approximately 2GHz. Fig. 3.25. shows the measured spectrum of before and after the IM3 suppression with CANE. Before suppression, the IM3 levels are 13.4 dB and 12.2dB lower than signal tones for the 1.995GHz carrier and 2GHz carrier respectively. After the IM3 cancellation, the intermodulation tones drop to 21dB and 20dB below signal tones respectively. Without reducing IM3 the drain efficiency is 49.6%; with IM3 suppression the drain efficiency is 47.8%. The in band signal power are approximately same before and after IM3 deduction. The experiment results reveal that the proposed method can successfully suppress the intermodulation terms for single or multi-carrier system, while maintaining

the in-band signal power and efficiency. The IM3 terms can be perfectly eliminated by placing them at nulls of the filter through designing the delay length. However, because the filter response is mainly determined by the baseband delaying at low frequency, even with some delay deviations from designed values the IM3 suppression can be sufficient enough. Typically, adding more channels can provide better filtering response and the performance will be further less sensitive to the IM3 position. Moreover, the phase and delay can be fully controlled in digital domain, one can easily vary the filter behavior to achieve desired IM3 suppression.

Note that the baseband delay length is independent to carrier frequency, therefore the filter behavior can be applied to arbitrary RF frequency and broadband delay lines are unnecessary. The other benefit of the proposed system is that all the branches share the same hardware units, such as PAs, I/Q mixers, which allows the system to be easily fabricated.

3.9 Summary

This chapter presents a discussion of CANE technique with theory, simulation and experiment. A two PAs combining module and a four PAs combining modules are fabricated and tested. The experimental results prove that CANE can provide a digitally baseband controlled reconfigurable RF filter in the bitstream modulated transmitter. The proposed technique provides an effective quantization noise filter as a complementary method to conventional physical output filter. The system power efficiency is preserved by utilizing the frequency domain load modulation. The measured power efficiency proves that the designed power combining scheme indeed recycles the noise power and maintains the system efficiency.

CHAPTER 4

Switched Mode Electrically Small Antenna

In a wireless transmitter, the antenna transmits signals into free space in the form of electromagnetic wave and indeed create a "wireless" link. To increase the communication capacity, the transmitter antenna is required to efficiently radiate signal over wider and wider bandwidth. Nowadays the dimensions of electronic devices are getting smaller and compact antenna is highly demanded. However, once the antenna size is much smaller than the wavelength, the radiation quality factor Q_{rad} becomes very high and limits the antenna radiation capability. This chapter firstly discusses the fundamental limits of the electrically small antenna, then introduces a switched mode antenna system called direct antenna modulation which helps the antenna overcome the the quality factor limitation.

4.1 Fundamentals of antenna

In a antenna system, the quality factor is an essential factor that describes the radiation performance. Generally, the quality factor is defined as:

$$Q = \omega \frac{Averag\ Energy\ Stored}{Power\ Disspation} = \omega \frac{W_m + W_e}{P_L} \tag{4.1}$$

For a resonating antenna, the radiation quality factor is defined as:

$$Q_{rad} = \frac{2\omega \max\{W_m, W_e\}}{P_{rad}} \tag{4.2}$$

W_m and W_e are the average stored magnetic energy and electric energy respectively. P_{rad} is the radiating power. In the equivalent circuit model of antenna, the radiating power is represented by the power consumed by a radiation resistance R_{rad} when the antenna is fed

with current I:

$$R_{rad} = \frac{2P_{rad}}{I^2} \tag{4.3}$$

Ideally, if the antenna is well matched, all the maximum available power from signal source ought to be transmitted from the antenna. However, the undesired ohmic resistance R_{ohmic} in the circuit consumes extra power. Assuming the antenna is matched, the antenna radiation efficiency can be defined as:

$$\eta = \frac{R_{rad}}{R_{rad} + R_{ohmic}} \times 100\% \tag{4.4}$$

In addition, let the power dissipate on R_{ohmic} be denoted by P_{ohmic}, we can define the loss quality factor Q_{loss}

$$Q_{loss} = \frac{2\omega \max\{W_m, W_e\}}{P_{loss}} \tag{4.5}$$

The total quality factor of the entire resonating antenna can be given by:

$$\frac{1}{Q_{total}} = \frac{1}{Q_{rad}} + \frac{1}{Q_{loss}} \tag{4.6}$$

In antenna design, we want to deliver more power on the radiation resistance and minimize power dissipation on the ohmic resistance. Note that the antenna radiation efficiency can be written in terms of quality factor:

$$\eta = \frac{Q_{total}}{Q_{rad}} \times 100\% \tag{4.7}$$

In other words, a smaller Q_{rad} and a larger Q_{loss} are preferred.

Note if the antenna is not matched to the source, part of the signal power is reflected back and the system radiation efficiency can be lower.

4.1.1 Chu's Limit

Unfortunately, in the electrically small antenna system, the lower bound of the radiation quality factor is constrained. According to Chu's limit [28–30], let the antenna dimension be a and the free space wavelength of the EM wave be λ, the lower bound of Q_{rad} is :

$$Q_{rad} \geq \frac{1}{(ka)^3} + \frac{1}{ka} \tag{4.8}$$

For electrically small antenna, as its size is much smaller than the wavelength, i.e,

$$ka << 1 \tag{4.9}$$

However, equation (4.7) shows that the radiation quality factor is inversely proportional to the cube of ka. So the radiation quality factor of such electrically small antenna is expected to be a large number. The high quality factor implies that the stored energy of the antenna is much stronger than the power radiated out. In other words, the radiation resistance gets smaller as the antenna size shrinks. Once the R_{rad} is smaller than R_{ohmic}, the majority of power from the source is wasted on the ohmic loss and the radiation becomes very inefficient.

People have proposed many revised models [31] of different electrically small antenna and obtained a tighter bound of Q_{rad}. But fundamentally the minimum available Q_{rad} of a three-dimensional antenna structure is constrained by the factor of $1/(ka)^3$.

4.1.2 Bandwidth and efficiency product limit

Because the radiation resistance is intrinsically small, another approach to improve the radiation efficiency is by minimizing the ohmic loss or increasing the loss quality factor Q_{loss}. However, according to equation (4.6), the large Q_{rad} and Q_{loss} lead to a high total quality factor. This means that the bandwidth of the antenna is limited. Typically, for a narrow band system, the fractional bandwidth is inversely proportional to Q, i.e,

$$BW \propto \frac{1}{Q_{total}} \tag{4.10}$$

Actually in some tests, the inverse of fractional bandwidth is used to indirectly evaluate the quality factor of a system. According to equation (4.7), if we rewrite the total quality factor as $Q_{total} = \eta \times Q_{rad}$, and substitute into (4.10), then,

$$(BW \times \eta) \propto \frac{1}{Q_{rad}} \tag{4.11}$$

This means that the product of the antenna bandwidth and radiation efficiency is proportional to inverse of the radiation quality factor. From here, we can see the radiation quality factor is the fundamental limitation of the antenna performance. In electrically small antenna system, the high Q_{rad} reveals that the antenna cannot transmit a broadband signal

with high efficiency. Even for an ideal antenna, once its dimensions are much smaller than wavelength, the available bandwidth is intrinsically narrow.

From its physics inside, the Q_{rad} limitation means that the radiating power is linearly proportional to the stored energy. The reason causes the narrow bandwidth is that the antenna has to charge or discharge its strong reactive field before it can efficiently radiate power. In the equivalent circuit model of the antenna, the high Q refers to a long response time. But if the broadband signal changes faster than the antenna charging or discharging procedure, the antenna won't be able to track the input signal.

Besides the radiating antenna system, near field communication link also suffers similar quality factor limitation. A high quality factor usually refers to high power transfer efficiency, but results in very narrow band. Therefore trade-off between power and bandwidth is needed to achieve the optimum capacity in conventional near field communication.

4.2 Direct Antenna Modulation

4.2.1 Principle

However, such high Q limitation is applied to a linear antenna system. On the other hand, if the radiating power is decoupled to the reactive energy, the antenna bandwidth might be no longer constrained. Direct antenna modulation (DAM) is proposed under this principle. Direct Antenna Modulation (DAM) has been proposed to overcome the bandwidth limitation without reducing the radiation efficiency. Different from the conventional time-invariant linear system, DAM employs time varying electromagnetic boundary conditions such that limitation of the bandwidth by Q is no longer applied.

In DAM system, a switch module is employed to directly modulate RF signal on the antenna. For example, Fig. 4.1 shows the diagram of a On/Off keying DAM with a electrically small dipole antenna. Due to the strong reactive energy stored in the near field, the electrically small antenna usually does not resonate by itself and its fundamental mode behaves like a lumped component. An extra reactive component is required to match the antenna.

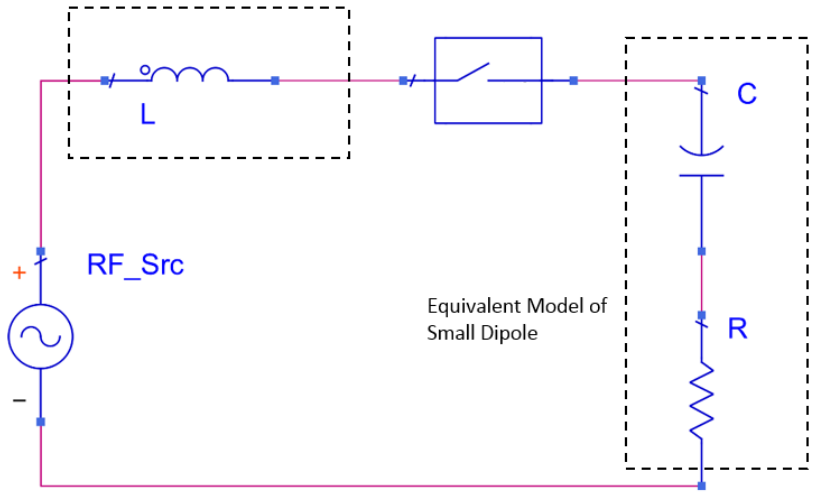

Figure 4.1: Schematic off DAM with electrically small dipole

For an electrically small dipole, the fundamental mode is similar to a capacitor; while for electrically loop antenna, it operates more like a lumped inductor. However, actual antenna has multiple radiation modes and all of them contribute to the radiation behavior. But for electrically small antenna, the fundamental mode dominates the others. So for simplicity, the small dipole in Fig 4.1 is modeled as a capacitor in series to a radiation resistor, which is matched with a lumped inductor. In the resonating status, the stored energy is bouncing back and forwards between the antenna and its matching network.

In Fig 4.1, a switch is used to turn the antenna on and off and create two symbols. When the antenna is turned on, it radiates sinusoidal wave into free space and transmits symbol "1"; when the antenna is turned off, it should stay in an electric static mode, which represent symbol "0". However, to indeed decouple the reactive energy and radiated power, the switching operation has to be at the moment when all the reactive energy is stored in the antenna, or when the current flowing in the circuit is zero. For the OOK modulation, when the antenna is switched off at zero current moment, the voltage across the capacitor reaches maximum. In other words, all of the reactive energy is stored inside and around the small dipole in a static electric field. During the "off" period, no current is allowed to flowing through the antenna, so no fundamental energy loss appears. Then after one period of carrier,

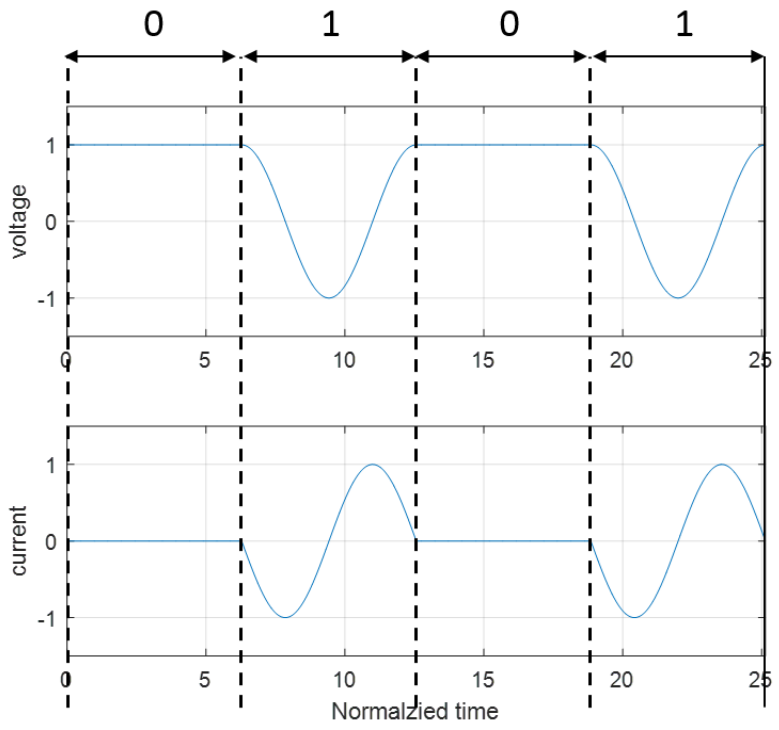

Figure 4.2: Voltage and Current waveform of OOK with DAM in electrically small dipole

if the antenna is switched on, it can immediately resonate with the inductor and radiate power without any response time. Fig 4.2 demonstrates the voltage and current waveform in this OOK modulation. In other words, if the switching rate is equal to the carrier frequency, the DAM system can obtain 100% fractional bandwidth for OOK modulation. However, if the switching condition is not followed, the energy loss from higher order resonating mode may cause additional charging/discharging of stored energy and limits the bandwidth.

On the contrary, the electrically small loop antenna can be modeled as a lumped inductor. When the voltage across the antenna is zero, or the current flowing through it reaches maximum, all the reactive energy is stored in the antenna as magnetic field. So for applying DAM with electrically small loop, the zero voltage switching condition must be satisfied.

4.2.2 Review of DAM

Previously, DAM has been applied to various antenna system. The first DAM idea was proposed in 1962 by J.Galejs [32], which discussed the principle of OOK modulation with

DAM concept electrically small dipole. J. Xu *et,al* [33–36] also proposed the similar technique and developed the theorem of switching conditions. In [34], finite-difference time-domain (FDTD) method has been used to simulate the waveform of the voltage, current and far field in OOK DAM system. DAM concept has also been used in near field communications [37].

But so far, DAM has only been used to generate simple digital modulation scheme, such as OOK. Because OOK can easily satisfy the zero voltage or zero current switching conditions. However, the other types of digital modulation schemes, such as QPSK and FSK, have to be modified to comply with the switching conditions.

In addition, as DAM leverages on the switches in antenna circuit, the requirement of switch devices is very stringent. Especially, the switching speed is the bottleneck of DAM system. For example, a long rise/fall time may cause discontinuous voltage or current waveform during the transition between two different symbols and creates spikes in the waveform and signal distortions. It also results in extra energy dissipation and efficiency degradation. So far DAM is limited to low frequency application.

CHAPTER 5

Development of DAM

5.1 Phase Modulation with DAM

In DAM system, the switching conditions are the most fundamental requirements to overcome the quality factor limits. But they also limit the ways of modulations and only simple modulation scheme such as OOK can be directly implemented in DAM. However, OOK is only "1-bit" modulation scheme and its spectral efficiency is poor. Although DAM enables an ultra wide band communication link, the frequency resource is not fully utilized. To transmit more information with same symbol rate, higher order digital modulations, such QPSK and 64QAM, are highly demanded.

Note that OOK can be regarded as an amplitude modulation, the phase of the reactive energy in stored in antenna is kept as constant. But to achieve higher order modulation, phase modulation is needed. Unfortunately, according to the DAM switching conditions, the symbol transition can only appear when the antenna is fully charged. In other words, the phase of the stored energy cannot be modulated.

However, if the antenna is switching between multiple sets of matching circuits at the moment when the reactive energy is stored completely outside the antenna, the stored energy will not be disturbed and phase modulation becomes possible. One potential solution is using the matching network to store the reactive energy. But it requires the matching network to keep the energy when it is switched off. In near field communications, this requirement can be easily implemented because the matching network in NFC is essentially a complementary reactive component to the antenna. For example, in a magnetic field coupled NFC link, the matching network basically is a capacitor which resonant the coupled loop at desired

frequency. So if we let the loop switch between two capacitors which are fully charged but with opposite voltage, a Binary Phase Shift Keying (BPSK) modulation can be achieved.

5.1.1 BPSK

Fig. 5.1 shows the diagram of proposed BPSK modulation with DAM in a loop antenna system. First of all, the electrically small loop antenna is simplified to a lumped inductor. A SPDT switch controls the inductor switching between two same capacitors. The two capacitors are connected to two RF source with 180 degree phase difference. Before enabling the whole system, the capacitors are pre-charged with opposite voltages respect to the source phase. Now the symbol transition moment is when the current flowing through the antenna is zero.

If the antenna is connected to C_1, they forms a sinusoidal wave with phase of 0 degree. During this time, the right terminal of capacitor C_2 is terminated by open circuit. So the charges on C_2 remain constant and its pre-charged energy is not lost. When the antenna is switched to the lower branch at zero current moment, it sees continuous current and voltage waveform and starts resonate with C_2 immediately, but the phase of the signal is opposite.

However, BPSK is still a "1 bit" modulation. But the idea of BPSK can be utilized to create higher order phase modulations. In addition, when one of the capacitor is switched off, it is terminated by an open circuit to preserve the charges on it. So the SPDT switch used in here must be reflection type and presents high impedance to the turned off branch.

5.1.2 QPSK

However, the conventional phase modulation techniques such as QPSK do not obey either zero voltage or zero current condition at the symbol transition moment, thus they have to be modified to fit into the operating conditions of DAM [38].

Note that in the antenna resonator if the switching moment is chosen at zero current, voltage across capacitor must reach its positive or negative maximum, corresponding to phase of 0 or 180 degree respectively. This implies that Binary Phase Shifted Keying (BPSK) can

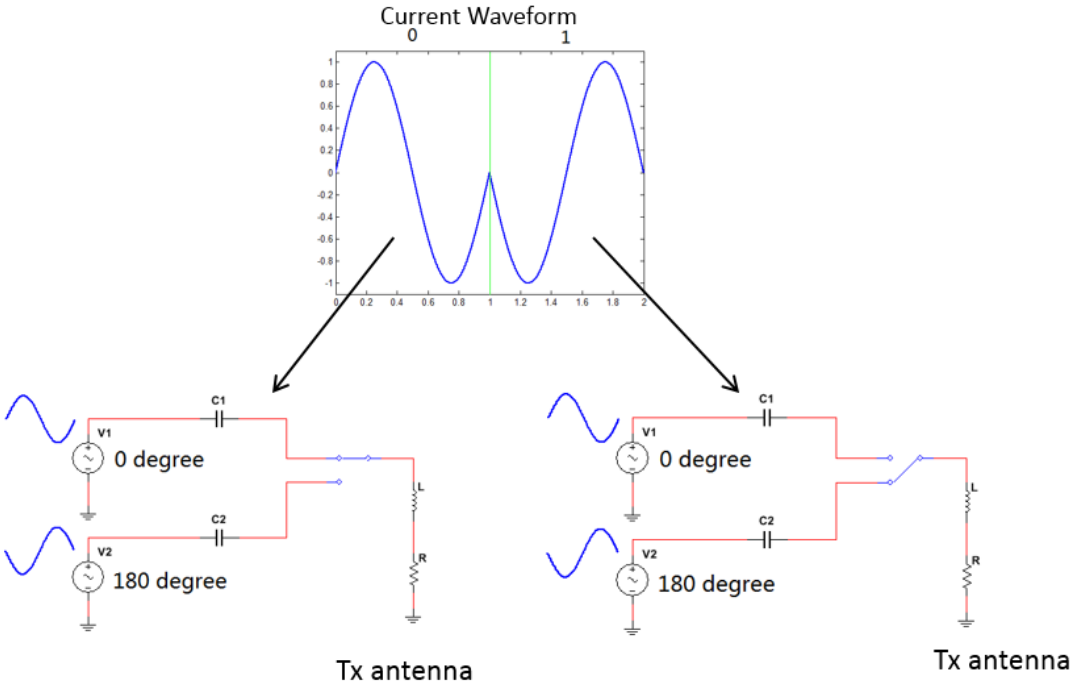

Figure 5.1: Diagram of BPSK with DAM in electrically small loop antenna system

be easily accomplished by including a differential switches pair to initialize the capacitor voltage at the switching moment. In addition, if switches short the inductor to ground at zero current moment, the capacitor voltage is being maintained as a constant, at its either positive or negative maximum. Therefore, retarding the starting point of a sine wave by a quarter of carrier period without disturbing the capacitor voltage by shorting the inductor to the ground creates an additional 90 degree phase shift, by which the four quadrature phases can be generated. The proposed QPSK waveform is shown in Fig. 5.2.

Basically, each of the four phase bit waveforms represents the current through the transmitting loop antenna, including a full period of sine wave with 0 or 180 degree phase, and a zero value gap with length of a quarter of full period before or after, providing four possible phase terms in 0, 90, 180, 270 degree. Switching always occurs at the zero current moment, which is the hard requirement of this DAM scheme. The initial voltage of the capacitor is controlled by additional switches to be either positive or negative. The modulator block diagram is shown in Fig.5.3, which illustrates the concept of forming these waveforms. An

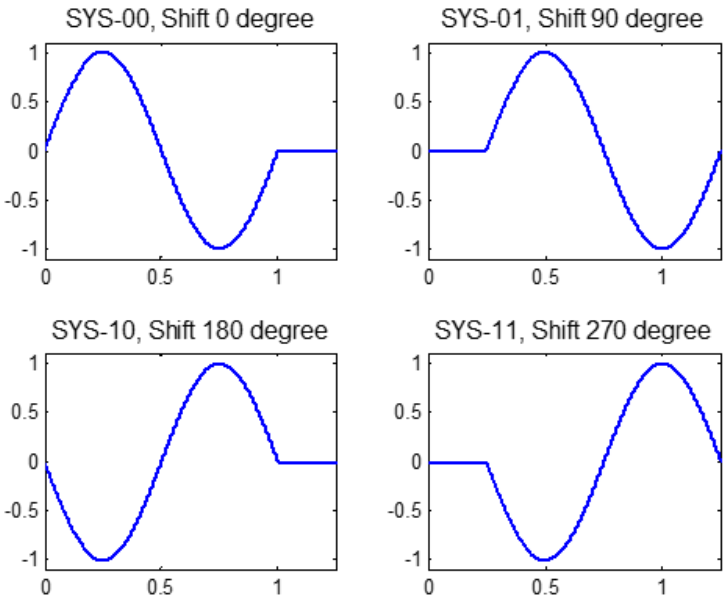

Figure 5.2: Symbols of modified QPSK for DAM.

example of voltage and current waveform of the modified QPSK is shown in Fig. 5.4. Due to the existance of quarter cycle zero current gaps, the symbol rate of his modulation approaches 75% of carrier frequency, while the total bit rate is almost 150% of the carrier frequency due to the doubled spectral efficiency with QPSK.

To validate the concept, A NFC system with the proposed modulation technique is set up and simulated in ADS. The NFC receiver is modeled as a coupled inductor to capture resonating magnetic field generated by the transmitter. A symbol rate of 10.848MbS/S is

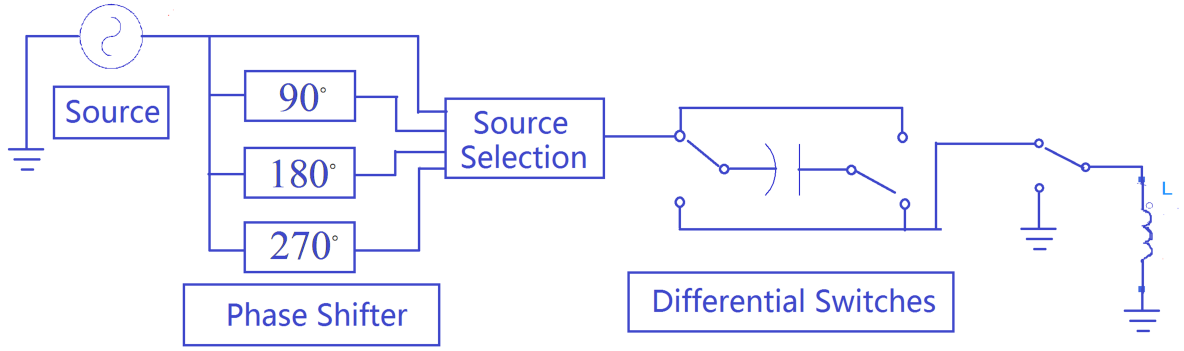

Figure 5.3: Time-domain waveform of the transmitting current

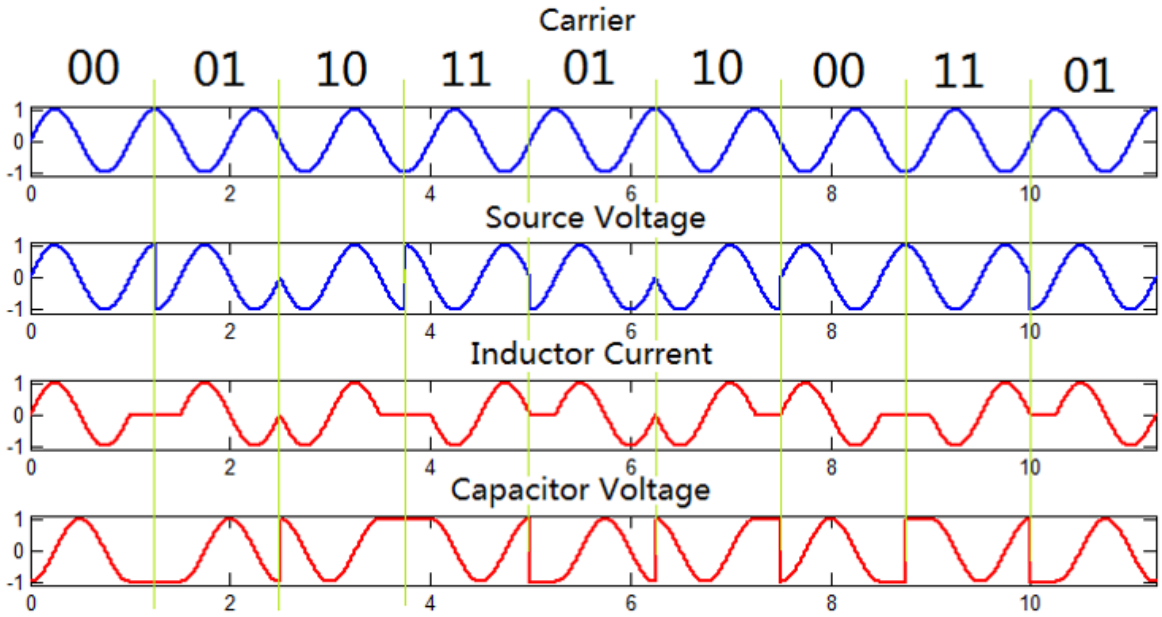

Figure 5.4: Time-domain waveform of the transmitting current

used over a carrier frequency of 13.56MHz. The eye diagrams of the received waveform with the DAM QPSK and the traditional QPSK modulations are shown in Fig.5.5. Note that the figure displays an opened eye for the scheme with DAM while the "eye is shut for traditional modulations. The data rate for the DAM scheme with the proposed QPSK modulation technique is thus 21.686Mbits/S.

5.2 Frequency Modulation with DAM

In above cases, the antenna is switched either between an electrostatic statue and a dynamic radiating state, or between dynamic status with different phases but in one frequency. However, if the antenna is switching between two sets of matching circuits at different frequency, a frequency shift keying modulation can be applied with DAM.

In the proposed FSK DAM system, a set of different reactive components is employed so the antenna can radiate at different frequencies and thus a frequency shift keying modulation can be achieved. For example, Fig.5.6 shows the diagram of the proposed FSK modulation

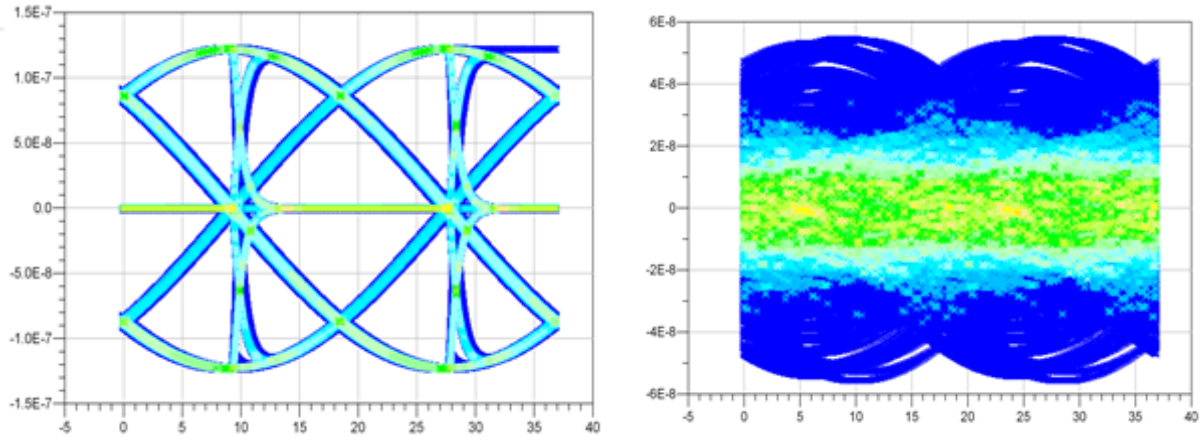

(a) (b)

Figure 5.5: Eye diagram of the received signal for the same set up except in the transmitter.(a) QPSK with DAM is used (b) Traditional QPSK modulation is used.

with DAM for a loop antenna. In this system, the electrically loop antenna is simplified as a lumped inductor. The antenna is switching between two capacitor C_1 and C_2 by a SPDT switch. and resonating between two frequencies f_1 and f_2. To meet the zero voltage switching condition, the two capacitor values are selected to match:

$$f_2 = N \times f_1 \tag{5.1}$$

where N is a positive integer. For example, if $f_2 = 2f_1$, the two capacitor should satisfy $C_1 = 4C_2$. Fig 5.7 shows the detailed operation principle of FSK with DSM. Let the symbol "0" be represented by one cycle of carrier "f_1", and symbol "1" be represented by two cycles of carrier "f_2" Then the symbol rate is equal to f_1. If the antenna is switched to C_1, symbol "0" is created. During this period, the voltage across C_2 is kept as zero, which means that no reactive energy is stored inside. Note that to meet the zero voltage switching condition, each symbol always starts and ends at zero voltage moment. So after one period of symbol, if the antenna is switched to C_2, then symbol "1" is created. Meanwhile, the voltage across "C_1" becomes zero. Because the boundary condition at transition moment between two different symbols is continuous, no charging or discharging of the reactive energy appears in the switching operations. So the bandwidth is no longer limited by the quality factor. Fig.5.8 shows a simulation setup of the proposed FSK DAM system in Keysight Advanced

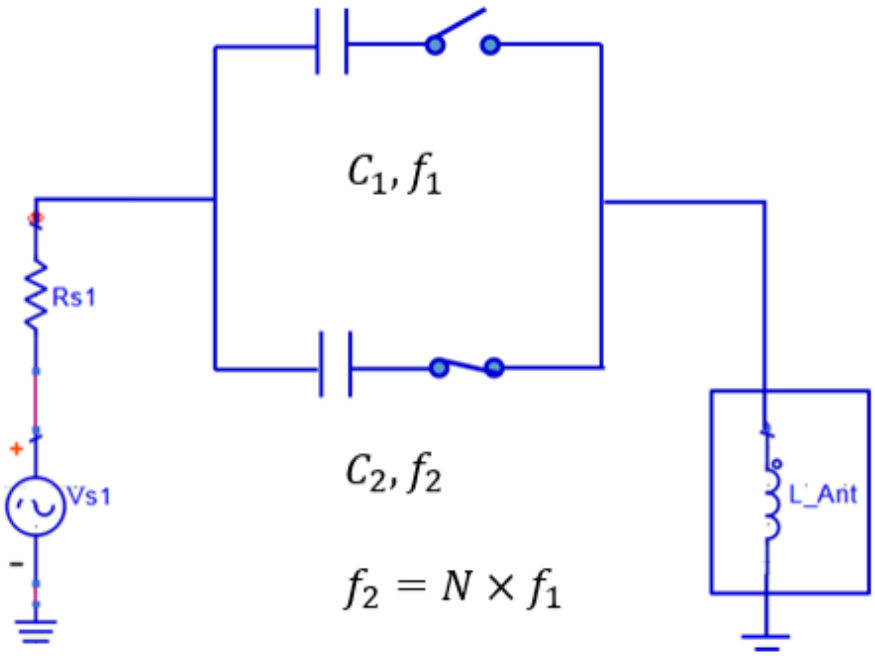

Figure 5.6: Diagram and Binary FSK with DAM

Design System (ADS). A loop antenna is modeled as an inductor, which can be resonating with two capacitors C_1 and C_2 at 1MHz and 2MHz respectively. An ideal SPDT switch is used to control the modulation. A transformer shown in the schematic is used to match the radiation resistance of the antenna to the signal source.

Fig 5.9 shows the simulation result of the proposed system. The top figure shows the simulated current waveform flowing through the antenna. The switching rate in this simulation is 1MHz, and we can observe that the current waveform clearly exhibits two patterns which represents "0" or "1". The bottom two figures shows the simulated S11 for two resonate mode. The quality factors of the resonating antenna at 1MHz and 2MHz are 22 and 45 respectively, which provides -5dB bandwidth about 45KHz. However, with DAM the symbol rate can be as high as 1MSps, which is more than 20 times of the physical bandwidth.

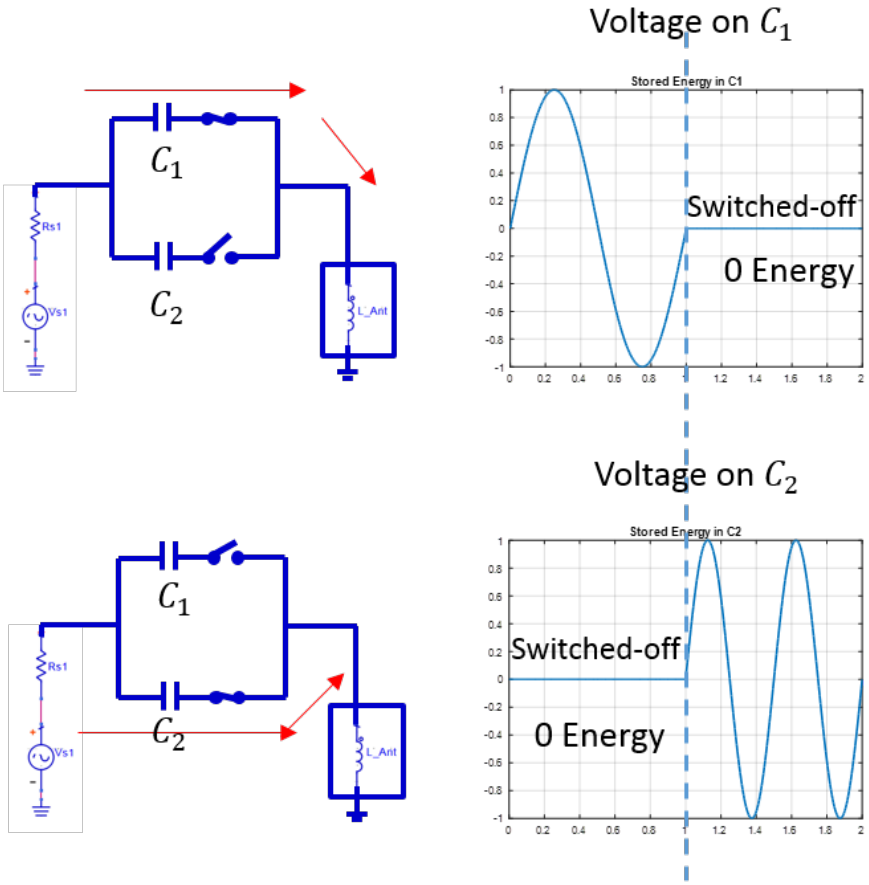

Figure 5.7: Operation Principle of FSK DAM

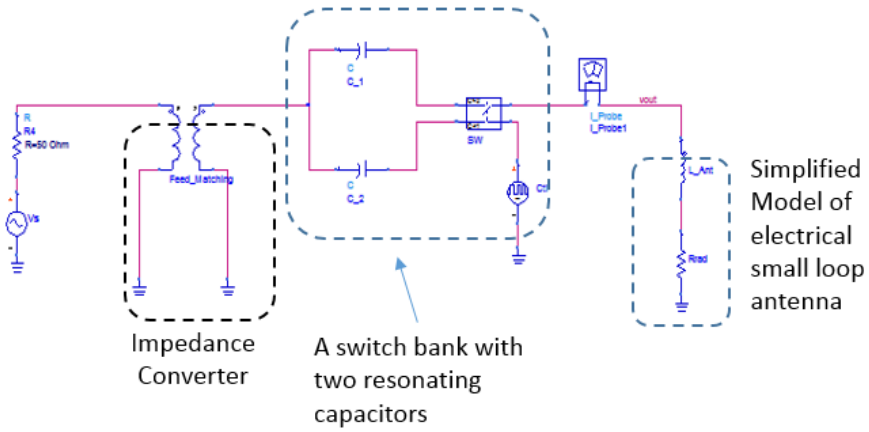

Figure 5.8: Simulation setup of FSK DAM in ADS.2016

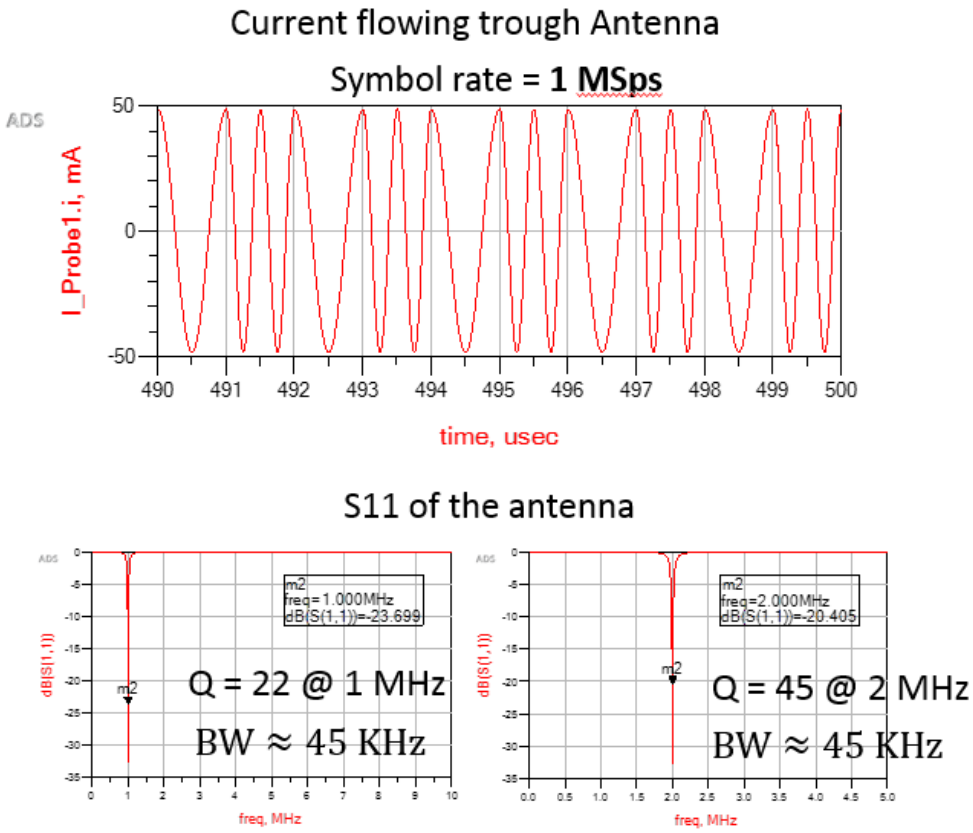

Figure 5.9: Simulation result of FSK DAM in ADS2016

5.3 Practical Implementation of DAM

5.3.1 Challenges in DAM

DAM utilizes switches to modulate signal directly on the electrically small antenna and decouples the stored energy and radiate power. However, this brings stringent requirement of the switches. First, the turning on resistance of the switch must be as small as possible to preserve the system power efficiency. Second, the turning-off status of the switch cannot present large parasitic output capacitance, otherwise the resonating frequency is shifted from desired value. In addition, if the amount of energy stored in this parasitic capacitor is too strong and not well synchronized with the energy in the rest of the circuits, the switching speed is limited and non-perfect switching behavior may cause extra power dissipation.

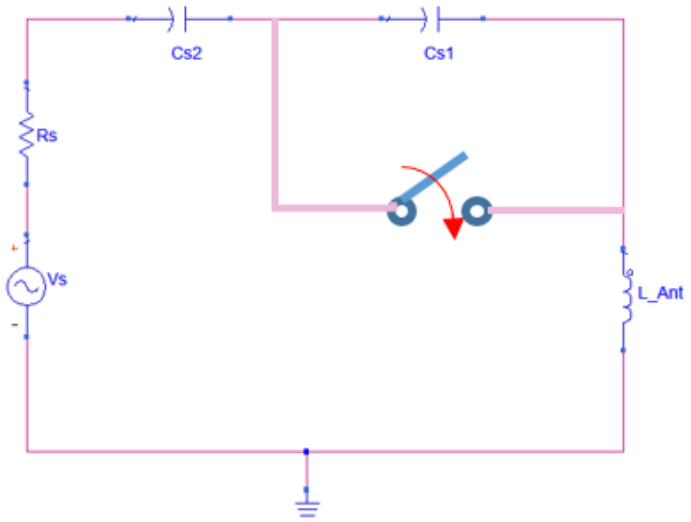

Figure 5.10: Modified FSK with DAM

Third, as the switch is placed in a resonating circuit path, it must be able to handle high voltage or high current swing. This special requirement of switches makes DAM difficult to practically implemented, especially for high frequency. But in some application at low frequency band, such as in VLF band, the system has to rely on electrically small antenna. Since at this frequency, deployment of DAM does not require very high switching rate, DAM can utilize current commercial switches to help break the bandwidth and efficiency limit.

5.3.2 Modified FSK

In fact, to overcome some of the non-perfect switching issues, a modified FSK with DAM is proposed. Fig.5.10 shows the schematic of the modified FSK scheme. Rather than let the antenna switch between two capacitors, two capacitors are connected in series but one of them is in parallel with a SPST switch. When the switch is turned on, the capacitor "C_s1" is bypassed and the antenna is resonating with capacitor "C_s2". If the switch is turned off, ideally the antenna is linked to the two series capacitors. In reality, the turning off capacitance of the switch involves in the resonating circuits. However, the capacitor "C_s1" can be tuned to absorb the parasitic capacitance and force the LC tank to resonate at desired frequency. Fig 5.11 shows the details of the operation principle. For the turning on status,

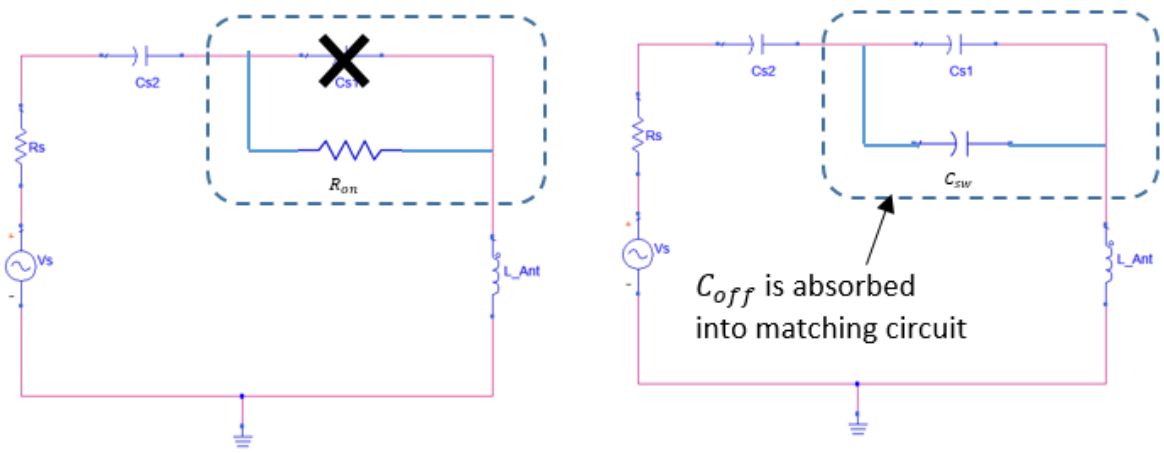

(a) (b)

Figure 5.11: Operation principle of the modified Binary FSK with DAM. (a) when the switch is turned on CANE (b) when the switch is turned off

the C_s1 is in parallel to the turning on resistance $R_{on}t$. If the insertion loss of the switch is negligible, voltage across C_s1 is approximately zero. Then the resonating frequency for symbol "0" is determined by:

$$f_0 = \frac{1}{2\pi\sqrt{L_{ant}C_{s2}}} \tag{5.2}$$

For the turning off status, the total capacitance in series to the antenna is:

$$C_{total} = \frac{C_{s2}(C_{s1} + C_{sw})}{C_{s1} + C_{s2} + C_{sw}} \tag{5.3}$$

where C_{sw} is the turning off capacitance of the switch. Then the resonant frequency of symbol "1" is:

$$f_1 = \frac{1}{2\pi\sqrt{L_{ant}C_{total}}} \tag{5.4}$$

To satisfy the zero voltage switching condition, let $f_1 = Nf_0$, then C_{s1} needs to be tuned to:

$$C_{s1} = \frac{C_{s2}}{N^2 - 1} - C_{sw} \tag{5.5}$$

Note that a small C_{sw} is the fundamental requirement in DAM. If the parasitic capacitor is too large, the proposed system may not obtain a valid solution for desired frequency.

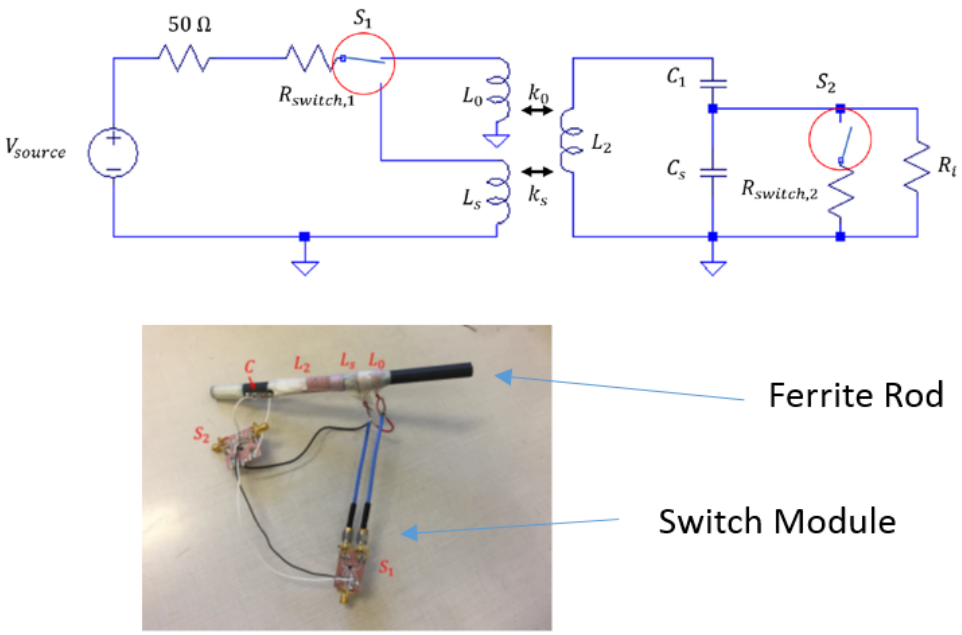

Figure 5.12: Schematic and picture of the modified FSK DAM

5.3.3 Experiment

Based on the modified FSK with DAM, a loop antenna for near field communication is fabricated and tested. Fig 5.12 shows the picture of the antenna. Two primary coils and one secondary coils are winded on a ferrite rod. The secondary coil is used to transmit the signal, the two primary coils are used to match the source impedance. The ferrite core helps to obtain a high Q system. Two capacitors and a switch module are used to form a FSK scheme.

The system is tuned to resonate at 28KHz and 56KHz, with quality factor of 63 and 173 respectively. The measured bandwidth is 320Hz at the lower frequency and 440Hz at the higher frequency. A receiving loop is used to capture the transmitted signal. Fig 5.13 shows the measured received waveform.

In the top figure, the symbol rate is selected to be 14KHz. Symbol "0" carries two periods of the 28KHz sinusoidal wave and Symbol "1" is represented by four periods of 56KHz wave. In the bottom figure, the symbol period is doubled, so the symbol rate is 7KHz. In both cases, the symbol rate is much greater than the antenna physical bandwidth.

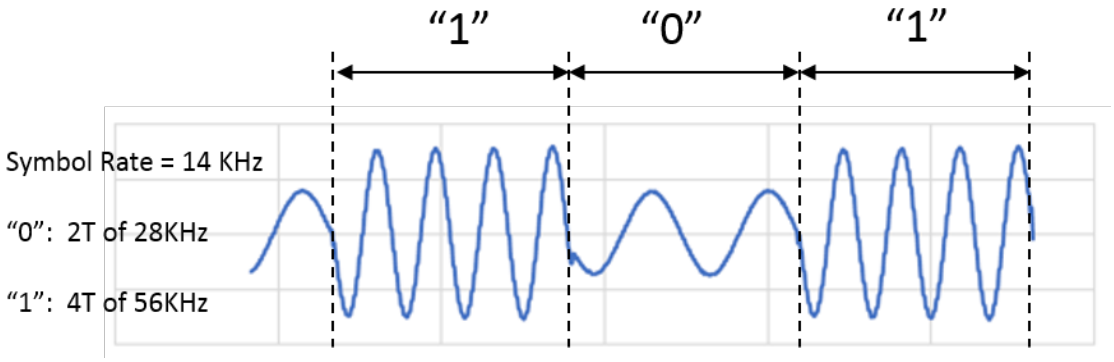

(a)

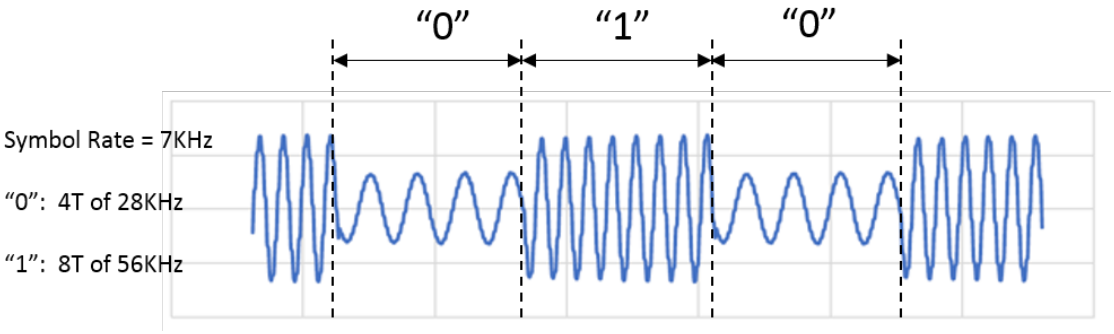

(b)

Figure 5.13: Measured received waveform from FSK with DAM.(a) Symbol rate = 14KHz (b) Symbol rate = 7KHz

The switch control signal is adjusted to impose zero voltage switching. From the waveform, every symbol transition moment has approximately zero crossing. In addition, because the parasitic capacitor of the switches are absorbed into the matching circuits, the switching quality is much better than previous OOK case [37].

Note that the magnitude of the lower frequency signal is half of the magnitude of the higher frequency signal. This is because the receiver loop detects the variation of magnetic field generated by the transmitter, while the frequency becomes a multiplier to the differentiate of the waveform. So the ratio of the two magnitude is same as the ratio of the frequency.

CHAPTER 6

Conclusion

In this research, digitally enhanced switched-mode transmitter architecture has been developed. In bitstream modulated transmitter, both theory and experiment result prove that Channelized Active Noise Elimination (CANE) technique can be a software-controlled, robust and flexibly tunable filter solution. In the electrically small antenna system, Direct Antenna Modulation (DAM) surpass the bandwidth limit by the high quality factor. A newly proposed DAM frequency shift keying (FSK) is developed to synthesize the parasitic components of switches with the matching circuit to improve the switching quality and signal integrity

REFERENCES

[1] Arun Jayaraman, PF Chen, G Hanington, L Larson, and P Asbeck. Linear high-efficiency microwave power amplifiers using bandpass delta-sigma modulators. *IEEE Microwave and guided wave letters*, 8(3):121–123, 1998.

[2] Yuanxun Wang. An improved kahn transmitter architecture based on delta-sigma modulation. In *Microwave Symposium Digest, 2003 IEEE MTT-S International*, volume 2, pages 1327–1330. IEEE, 2003.

[3] Alexandre Dupuy and Yuanxun Ethan Wang. High efficiency power transmitter based on envelope delta-sigma modulation (edsm). In *Vehicular Technology Conference, 2004. VTC2004-Fall. 2004 IEEE 60th*, volume 3, pages 2092–2095. IEEE, 2004.

[4] Tsai-Pi Hung, Jeremy Rode, Lawrence E Larson, and Peter M Asbeck. Design of h-bridge class-d power amplifiers for digital pulse modulation transmitters. *IEEE Transactions on Microwave Theory and Techniques*, 55(12):2845–2855, 2007.

[5] M Tanio, S Hori, M Hayakawa, N Tawa, K Motoi, and K Kunihiro. A linear and efficient 1-bit digital transmitter with envelope delta-sigma modulation for 700mhz lte. In *Microwave Symposium (IMS), 2014 IEEE MTT-S International*, pages 1–4. IEEE, 2014.

[6] Jinseong Jeong and Yuanxun Ethan Wang. A polar delta-sigma modulation (pdsm) scheme for high efficiency wireless transmitters. In *Microwave Symposium, 2007. IEEE/MTT-S International*, pages 73–76. IEEE, 2007.

[7] Joon Hyung Kim, Sung Jun Lee, Jae Ho Jung, and Chul Soon Park. 60% high-efficiency 3g lte power amplifier with three-level delta sigma modulation assisted by dual supply injection. In *Microwave Symposium Digest (MTT), 2011 IEEE MTT-S International*, pages 1–4. IEEE, 2011.

[8] Shu-Hsien Liao and Yuanxun Ethan Wang. High efficiency wcdma power amplifier with pulsed load modulation (plm). *IEEE Journal of Solid-State Circuits*, 45(10):2030–2037, 2010.

[9] Yonghoon Song, Rui Zhu, and Yuanxun Ethan Wang. An x-band pulsed load modulation transmitter with multilevel envelope delta–sigma modulations. *IEEE Transactions on Microwave Theory and Techniques*, 64(11):3643–3653, 2016.

[10] Yonghoon Song, Rui Zhu, and Yuanxun Ethan Wang. A pulsed load modulation (plm) power amplifier with 3-level envelope delta-sigma modulation (edsm). In *Power Amplifiers for Wireless and Radio Applications (PAWR), 2015 IEEE Topical Conference on*, pages 1–3. IEEE, 2015.

[11] Axel Flament, Antoine Frappe, Andreas Kaiser, Bruno Stefanelli, Andreia Cathelin, and Hilal Ezzeddine. A 1.2 ghz semi-digital reconfigurable fir bandpass filter with

passive power combiner. In *Solid-State Circuits Conference, 2008. ESSCIRC 2008. 34th European*, pages 418–421. IEEE, 2008.

[12] Shota Fujioka, Michiaki Kojima, Hironori Izumi, Yohtaro Umeda, and Osamu Takyu. Power-amplifier-inserted transversal filter for application to pulse-density-modulation switching-mode transmitters. In *Communications and Information Technologies (ISCIT), 2012 International Symposium on*, pages 239–244. IEEE, 2012.

[13] Ritesh Bhat and Harish Krishnaswamy. A watt-level 2.4 ghz rf i/q power dac transmitter with integrated mixed-domain fir filtering of quantization noise in 65 nm cmos. In *Radio Frequency Integrated Circuits Symposium, 2014 IEEE*, pages 413–416. IEEE, 2014.

[14] Yonghoon Song, Rui Zhu, and Yuanxun Ethan Wang. A x-band gan power amplifier with bitstream modulations and active noise filtering. In *Microwave Symposium (IMS), 2015 IEEE MTT-S International*, pages 1–3. IEEE, 2015.

[15] Yonghoon Song, Rui Zhu, and Yuanxun Ethan Wang. Active noise filtering for x-band gan transmitters with bitstream modulations. *IEEE Transactions on Microwave Theory and Techniques*, 65(4):1372–1380, 2017.

[16] Rui Zhu, Yonghoon Song, Y Ethan Wang, and Yuexing Li. A s-band bitstream transmitter with channelized active noise elimination (cane). In *Wireless and Microwave Technology Conference (WAMICON), 2015 IEEE 16th Annual*, pages 1–3. IEEE, 2015.

[17] Rui Zhu, Yonghoon Song, and Yuanxun Ethan Wang. Channelized active noise elimination (cane) with envelope delta sigma modulation. In *Silicon Monolithic Integrated Circuits in RF Systems (SiRF), 2015 IEEE 15th Topical Meeting on*, pages 55–57. IEEE, 2015.

[18] Rui Zhu, Yonghoon Song, and Yuanxun Ethan Wang. Suppressing transmitter intermodulations with channelized active noise elimination (cane). In *Microwave Symposium (IMS), 2015 IEEE MTT-S International*, pages 1–4. IEEE, 2015.

[19] Feipeng Wang, Donald F Kimball, Jeremy D Popp, Annie Hueiching Yang, Donald Y Lie, Peter M Asbeck, and Lawrence E Larson. An improved power-added efficiency 19-dbm hybrid envelope elimination and restoration power amplifier for 802.11 g wlan applications. *IEEE Transactions on Microwave Theory and Techniques*, 54(12):4086–4099, 2006.

[20] Feipeng Wang, Donald F Kimball, Donald Y Lie, Peter M Asbeck, and Lawrence E Larson. A monolithic high-efficiency 2.4-ghz 20-dbm sige bicmos envelope-tracking ofdm power amplifier. *IEEE Journal of Solid-State Circuits*, 42(6):1271–1281, 2007.

[21] Lawrence Larson. Rf and microwave hardware challenges for future radio spectrum access. *Proceedings of the IEEE*, 102(3):321–333, 2014.

[22] F Raab. Efficiency of outphasing rf power-amplifier systems. *IEEE Transactions on Communications*, 33(10):1094–1099, 1985.

[23] Henry Chireix. High power outphasing modulation. *Proceedings of the Institute of Radio Engineers*, 23(11):1370–1392, 1935.

[24] Nitesh Singhal, Haoxing Zhang, and Sudhakar Pamarti. A zero-voltage-switching contour-based outphasing power amplifier. *IEEE Transactions on Microwave Theory and Techniques*, 60(6):1896–1906, 2012.

[25] Sunbo Shim and Sudhakar Pamarti. A 1.85 ghz cmos power amplifier with zero-voltage-switching contour-based outphasing control to improve back-off efficiency. In *Microwave Symposium (IMS), 2015 IEEE MTT-S International*, pages 1–4. IEEE, 2015.

[26] William H Doherty. A new high efficiency power amplifier for modulated waves. *Proceedings of the Institute of Radio Engineers*, 24(9):1163–1182, 1936.

[27] Shinho Kim and Yuanxun Ethan Wang. Theory of switched rf resonators. *IEEE Transactions on Circuits and Systems I: Regular Papers*, 53(12):2521–2528, 2006.

[28] Lan Jen Chu. Physical limitations of omni-directional antennas. *Journal of applied physics*, 19(12):1163–1175, 1948.

[29] Harold A Wheeler. Fundamental limitations of small antennas. *Proceedings of the IRE*, 35(12):1479–1484, 1947.

[30] Roger F Harrington. Effect of antenna size on gain, bandwidth, and efficiency. *J. Res. Nat. Bur. Stand*, 64(1):1–12, 1960.

[31] HD Foltz and JS McLean. Limits on the radiation q of electrically small antennas restricted to oblong bounding regions. In *Antennas and Propagation Society International Symposium, 1999. IEEE*, volume 4, pages 2702–2705. IEEE, 1999.

[32] J Galejs. Switching of reactive elements in high-q antennas. *IEEE Transactions on Communications Systems*, 11(2):254–255, 1963.

[33] Xiaojing Xu, Hengzhen Crystal Jing, and Yuanxun Ethan Wang. High speed pulse radiation from switched electrically small antennas. In *Antennas and Propagation Society International Symposium 2006, IEEE*, pages 167–170. IEEE, 2006.

[34] Xiaojing Xu and Yuanxun Ethan Wang. Wideband pulse transmission from switched electrically small antennas. In *Radio and Wireless Symposium, 2007 IEEE*, pages 483–486. IEEE, 2007.

[35] Xiaojing Xu and Yuanxun Ethan Wang. Beyond the efficiency bandwidth limit with switched electrically small antennas. In *Antennas and Propagation Society International Symposium, 2007 IEEE*, pages 2261–2264. IEEE, 2007.

[36] Xiaojing Xu and Yuanxun Ethan Wang. Electrically small loop loaded printed dipoles for broad coverage. In *Antennas and Propagation Society International Symposium, 2008. AP-S 2008. IEEE*, pages 1–4. IEEE, 2008.

[37] Umar Azad and Yuanxun Ethan Wang. Direct antenna modulation (dam) for enhanced capacity performance of near-field communication (nfc) link. *IEEE Transactions on Circuits and Systems I: Regular Papers*, 61(3):902–910, 2014.

[38] Rui Zhu and Yuanxun Ethan Wang. A modified qpsk modulation technique for direct antenna modulation (dam) systems. In *Antennas and Propagation Society International Symposium (APSURSI), 2014 IEEE*, pages 1592–1593. IEEE, 2014.